

Optimal Beamforming Design for Multi-user MIMO Near-Field ISAC Systems with Movable Antennas

Nemanja Stefan Perović, *Member, IEEE*, Keshav Singh, *Senior Member, IEEE*, Chih-Peng Li, *Fellow, IEEE*, Octavia A. Dobre, *Fellow, IEEE*, and Mark F. Flanagan, *Senior Member, IEEE*

Abstract—Integrated sensing and communication (ISAC) has been recognized as one of the key technologies capable of simultaneously improving communication and sensing services in future wireless networks. Moreover, the introduction of recently developed movable antennas (MAs) has the potential to further increase the performance gains of ISAC systems. Although the gains of MA-enabled ISAC systems are relatively well studied in the far field, they remain almost unexplored in near-field scenarios. Motivated by this, in this paper we maximize the weighted sum rate (WSR) for communication users while maintaining a minimum sensing requirement in an MA-enabled near-field ISAC system. To achieve this goal, we propose algorithms that optimize the communication precoding matrices, the sensing transmit beamformer, the sensing receive combiner, the positions of the users MAs and the positions of the base station (BS) transmit MAs in an alternating manner for the considered ISAC system, for the cases where linear precoding and zero-forcing (ZF) precoding are employed at the BS. Simulation results show that using MAs in near-field ISAC systems provides a substantial performance advantage compared to near-field ISAC systems equipped with fixed antennas only. We show that the scheme with linear precoding achieves larger WSR for unequal users' weight rates, while the scheme with ZF precoding maintains an approximately constant WSR for all users' weight rates. Additionally, we demonstrate that the WSRs of the proposed schemes are highly dependent on the inter-antenna interference between different users MAs, and that the sensing performance is significantly more affected by the minimum sensing signal-to-interference-plus-noise ratio (SINR) threshold compared to the communication performance.

Index Terms—Optimization, near-field, movable antenna (MA), integrated sensing and communication (ISAC), weighted sum rate (WSR), sensing signal-to-interference-plus-noise ratio (SINR).

I. INTRODUCTION

Future wireless communication systems will have to support many new functionalities, among which high-precision sensing is one of the most important as it enables various environment-aware applications such as augmented reality and digital twins. A promising technology for implementing this functionality is that of integrated sensing and communication (ISAC) [2]; this refers to a design paradigm in which sensing and communication systems are integrated to efficiently utilize the shared spectrum and hardware resources, while offering mutual benefits [3]. Through collaboration that includes appropriate reuse of resources and information, ISAC enhances both sensing and communication capabilities, and provides flexible trade-offs between these two

N. S. Perović, K. Singh, and C.-P. Li are with the Institute of Communications Engineering, National Sun Yat Sen University, Kaohsiung 80424, Taiwan (e-mail: n.s.perovic@mail.nsysu.edu.tw, keshav.singh@mail.nsysu.edu.tw, cpli@mail.nsysu.edu.tw).

O. A. Dobre is with the Faculty of Engineering and Applied Science, Memorial University of Newfoundland, St. Johns, NL A1C 5S7, Canada (e-mail: odobre@mun.ca).

M. F. Flanagan is with the School of Electrical and Electronic Engineering, University College Dublin, Dublin 4, D04 V1W8, Ireland (e-mail: mark.flanagan@ieee.org).

A partial version of this work has been submitted to the IEEE International Conference on Communications 2026, Glasgow, Scotland, UK [1].

functionalities in different use cases [4]. Furthermore, due to the possibility of integrating new wireless technologies, such as radio-frequency identification (RFID) [5], unmanned aerial vehicles (UAVs) [6], and non-orthogonal multiple access (NOMA) [7], ISAC has attracted significant attention from both the academic community and industry.

In conventional systems, fixed-position antenna arrays are generally deployed in order to carry out communication and sensing tasks. In particular, multiple-input multiple-output (MIMO) technology is a promising solution for ISAC due to its ability to steer the communication and the sensing signals toward the desired directions, reducing the signal interference and thereby improving the overall system performance [8]. As a result, MIMO systems can offer enhanced sensing accuracy and/or channel capacity. Motivated by this, a significant research effort has been dedicated to exploring the problem of optimal antenna positioning in MIMO systems. An efficient algorithm for selecting a subset of transmit antennas that maximizes the channel capacity in a massive MIMO (mMIMO) array was presented in [9]. Another technique, known as sparse array synthesis, uses a flexible array structure to achieve different radiation pattern properties (e.g., desired pattern directivity, reduced power leakage) [10], [11]. However, the basic assumption underlying both of the aforementioned techniques is that the set of available antenna positions is fixed and discrete, which prevents the utilization of the full range of positions of the antennas in the array.

The recent development of metamaterials-enabled manufacturing of intelligent metasurfaces with densely packed tunable elements, which can dynamically control the propagation of radio waves, have potential to improve ISAC capabilities [12]. An element-wise closed-form optimization method for adjusting the reconfigurable intelligent surface (RIS) reflection coefficients for improving the sensing signal-to-interference-plus-noise ratio (SINR) and reducing the communication interference was proposed in [13]. In [14], the authors introduced a two-phase ISAC transmission protocol for an RIS-aided MIMO ISAC system, which can obtain almost the same communication performance as a system with perfect channel state information (CSI), while providing up to millimeter-level positioning accuracy. In [15], it was demonstrated that deploying an RIS can significantly improve the performance of cooperative multicell ISAC systems in reducing the transmit power, while achieving communication and sensing requirements. Optimization of an ISAC system equipped with an active RIS was presented in [16], where it was demonstrated that the use of an active RIS can provide significantly better performance compared to an ISAC system with a passive RIS. However, all of the designs mentioned above are based on fixed metasurface element positions and/or orientations once manufactured. In practical wireless systems with varying signal propagation environments, such fixed-position metasurfaces may

not fully exploit the spatial variation of wireless channels, which limits their degrees of freedoms (DoFs) in the spatial domain.

Recently, movable antennas (MAs) have emerged as a promising technology to further improve the effectiveness of ISAC by enabling the local movement of antennas at transmitters and receivers [17]. Different from conventional fixed antennas, MAs can adjust their placements to adapt to evolving channel conditions. Dynamic positioning of such antennas enables precise beamforming design, avoiding undesirable side lobes and reducing interference, which enhances data rate/reliability and sensing accuracy [18]. Therefore, superior performance can be achieved by MA systems using the same or even a smaller number of antennas compared to conventional fixed antenna arrays.

Motivated by this, a significant number of papers have studied the use of MAs in ISAC systems. In [19], the authors studied the Cramér-Rao lower bound (CRLB) for angle of arrival (AoA) estimation as a function of the MA positions in 1D and 2D antenna arrays, and proposed algorithms for its optimization. In [20], the CRLB was derived for angle estimation error in an MA-enabled ISAC system, and optimization algorithms were proposed for the cases where only transmit MAs are present, only receive MAs are present, and both transmit and receive MAs are present. Maximization of the weighted sum of the communication rate and the sensing mutual information (MI) in a bistatic ISAC system with an MA transmit array was considered in [21]. An optimization framework that maximizes the sensing SINR in a multi-user bistatic ISAC system, where MAs are deployed for adjusting the array responses at both the transmitter and the receiver of a base station (BS), was introduced in [22]. In [23], the authors proposed the design and optimization of an RIS-aided ISAC broadcast system with MAs at the BS under imperfect CSI for both sensing and communication channels. Practical gains achieved by using MAs with a discrete set of possible antenna positions in an ISAC system with a dynamic radar cross-section were analyzed in [24]. The use of an MA array on an UAV for enabling simultaneous information transmission and reliable feature sensing for low-altitude economy (LAE) applications was studied in [25].

In contrast to all of the aforementioned works that consider ISAC systems with MAs operating in the far field, the implementation of ISAC systems with MAs in the near field remains largely unexplored. One of the main challenges regarding near-field communications is providing a large number of DoF for which the required MA moving region has to be much larger than the apertures of conventional fixed antenna arrays. Moreover, near-field ISAC systems are generally expected to work in high frequency bands to provide large data rates and high sensing resolution, in which case all of the communication and sensing distances are less than the Fraunhofer/Rayleigh distance (i.e., the border between the near- and far-field regions) [26], [27]. For these reasons, most of previous studies on ISAC systems with MAs are not directly applicable to near-field scenarios. Moreover, there is a significant interest to fill in this gap and understand the fundamental performance of MA-based ISAC systems operating in the near field.

To the best of the authors' knowledge, there are only a few papers dealing with the design of such systems. In [28], the authors proposed a sensing-centric and a communication-centric design for near-field ISAC systems with rotatable MAs at the BS,

and demonstrated their performance advantage compared to fixed-position antennas and non-rotatable MAs. The maximization of the weighted sum of the communication and sensing rates in a full-duplex near-field ISAC communication system with MAs at the BS was studied in [29]. For the latter system, the MA positions were obtained by selecting from a predefined set of MA positions those that provide the largest value of the objective function. A deep learning (DL)-based optimization framework that maximizes the weighted sum rate (WSR) while ensuring the required sensing performance through CRLB constraints for an MA-enabled RIS architecture operating in the near field was proposed in [30].

Against this background, the contributions of this paper are summarized as follows:

- 1) We introduce an optimization framework for multi-user ISAC systems operating in the near field, where the BS transmitter and each user are equipped with multiple MAs. Within this framework, we formulate an optimization problem with the aim of maximizing the WSR while satisfying minimum sensing SINR requirements, for the cases of both linear and zero-forcing (ZF) precoding for the communication signals at the BS.
- 2) For the system with linear precoding, we propose an alternating optimization (AO) based algorithm to solve the formulated problem by decomposing it into multiple subproblems. To optimize the sensing receive combiner, we provide a closed-form solution. The communication precoding matrices are optimized using the successive convex approximation (SCA) method, which provides a tight concave lower bound on the achievable rate of each user. Using the same approach and employing semi-definite relaxation (SDR), we optimize the sensing transmit beamforming vector. Finally, the positions of the users' MAs are obtained via the projected gradient method (PGM), while the positions of the BS transmit MAs are optimized by the augmented Lagrangian method (ALM). A similar AO approach is proposed to solve the optimization problem for the system with ZF precoding. However, in this case the positions of the users' MAs are optimized by the ALM, since they also affect the sensing SINR.
- 3) We show through simulations that the proposed algorithms achieve significantly improved performance compared to benchmark schemes equipped with only fixed antennas, due to a larger number of DoF. Moreover, we demonstrate that a larger WSR for the scheme with linear precoding is obtained when the users' rate weights are unbalanced, while the WSR for the scheme with ZF precoding stays approximately constant irrespective of these rate weights. In systems with a low number of MAs per user, ZF precoding can provide the best WSR performance, while on the other hand this performance decreases significantly for a larger number of MAs per user due to larger inter-antenna interference between different users MAs. Finally, we demonstrate that the sensing performance for both precoding schemes in the considered ISAC system is significantly more affected by the sensing SINR threshold compared to the communication performance.

The rest of this paper is organized as follows. In Section II, we introduce the system model and formulate the optimization problem to maximize the WSR of an ISAC MIMO system with

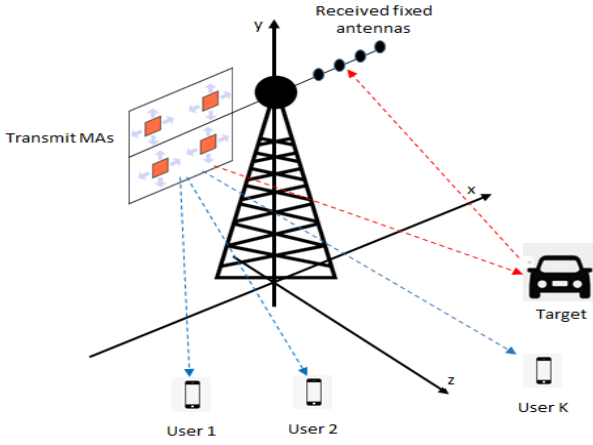


Fig. 1: System model for the proposed MA-aided near-field ISAC system.

MAs at the BS transmitter and at each user. In Section III, we propose and derive an algorithm to solve this optimization problem in the case of linear precoding. An algorithm to solve the same optimization problem in the case of ZF precoding is proposed in Section IV. In Section V, we present numerical WSR results for the proposed algorithms, and use these to illustrate their relative advantages. Finally, Section VI concludes this paper.

Notation: Bold lower and upper case letters represent vectors and matrices, respectively. \mathbf{I}_x is the identity matrix of size $x \times x$. $\text{Tr}(\mathbf{X})$, $\text{rank}(\mathbf{X})$, $\|\mathbf{X}\|$ and $|\mathbf{X}|$ denote the trace, rank, norm and determinant of matrix \mathbf{X} , respectively. $\mathbf{X} \succeq (\succ) \mathbf{Y}$ means that $\mathbf{X} - \mathbf{Y}$ is positive semidefinite (definite). $\mathbb{E}\{\cdot\}$ stands for the expectation operator. $\ln(\cdot)$ is the natural logarithm, and $(\cdot)^T$ and $(\cdot)^H$ represent transpose and Hermitian transpose, respectively. $\mathcal{CN}(\mu, \sigma^2)$ denotes a circularly symmetric complex Gaussian random variable with mean μ and variance σ^2 . $\Re(\cdot)$ and $\Im(\cdot)$ denote the real and imaginary part of a complex number, respectively. $\mathbf{X}(i, k)$ denotes the k -th element of the i -th row of matrix \mathbf{X} . $\mathbf{x}(i)$ denotes the i -th element of vector \mathbf{x} .

II. SYSTEM MODEL

In the considered MA-aided near-field ISAC system, a dual-functional BS is equipped with a transmit MA array, as shown in Fig. 1. This array with N_t antennas transmits the ISAC signal, which enables communication with K users and detection of a sensing target. Each of these MAs can be moved within a square transmit region which is denoted as C_t . In addition, the BS has a second antenna array with N_r fixed antennas, which receive the reflected echo signal from the sensing target. These two arrays are separated one from another so that the mutual coupling between antennas from different arrays is negligible. Each user is equipped with N_u receive MAs, which can be moved within the square region denoted as C_k .

To describe the geometry of the considered system, we establish a 3D Cartesian coordinate system, where the xz -plane represents the ground. The BS is placed at the origin with both of its antenna arrays in the xy -plane. The BS MA transmit region C_t has its center at $\mathbf{o}_t = [x_t, y_t, 0]^T$ and its side length is L_t . The coordinates of the m -th ($1 \leq m \leq N_t$) transmit antenna are given by $\mathbf{t}_m = [x_{t,m}, y_{t,m}, 0]^T$. The receive BS antennas are placed in a uniform linear array (ULA) parallel to the x -axis, with the midpoint at $\mathbf{o}_r = [x_r, y_r, 0]^T$ and a length of L_r . The

coordinates of the n -th ($1 \leq n \leq N_r$) receive antenna are $\mathbf{r}_n = [x_{r,n}, y_r, 0]^T$, where $x_{r,n} = x_r - L_r/2 + (n-1)L_r/(N_r-1)$. Without loss of generality, we assume the MA regions of all users are parallel to the xy -plane. For user k , the region C_k is of a square shape with the center at $\mathbf{o}_{u,k} = [x_{u,k}, y_{u,k}, z_{u,k}]^T$ and its side is denoted as a_k . The coordinates of the N_k MAs in C_k are collectively denoted as $\mathbf{q}_k = [(\mathbf{q}_{k,1})^T, (\mathbf{q}_{k,2})^T, \dots, (\mathbf{q}_{k,N_k})^T]^T$, where $\mathbf{q}_{k,b} = [x_{k,b}, y_{k,b}, z_{k,b}]^T \in C_k$ for $1 \leq b \leq N_u$. Finally, the position of the sensing target is specified as $\mathbf{s} = [x_s, y_s, z_s]^T$.

Since the users are located in the near-field region of the BS, the quasi-static spherical wave channel model is used for the relevant communication channels [26]. Accordingly, the channel between the BS and user k can be expressed as

$$\mathbf{H}_k = \rho_k \begin{bmatrix} e^{j\frac{2\pi}{\lambda}\|\mathbf{t}_1 - \mathbf{q}_{k,1}\|} & \dots & e^{j\frac{2\pi}{\lambda}\|\mathbf{t}_{N_t} - \mathbf{q}_{k,1}\|} \\ \vdots & \ddots & \vdots \\ e^{j\frac{2\pi}{\lambda}\|\mathbf{t}_1 - \mathbf{q}_{k,N_k}\|} & \dots & e^{j\frac{2\pi}{\lambda}\|\mathbf{t}_{N_t} - \mathbf{q}_{k,N_k}\|} \end{bmatrix}, \quad (1)$$

where λ is the wavelength and ρ_k is the free space path-loss.

Assuming that the target is also located in the near-field region of the BS, the sensing channel can be expressed as

$$\mathbf{G} = \rho_s \mathbf{f}_r \mathbf{f}_t^H, \quad (2)$$

where $\mathbf{f}_t = [e^{j\frac{2\pi}{\lambda}\|\mathbf{t}_1 - \mathbf{s}\|}, \dots, e^{j\frac{2\pi}{\lambda}\|\mathbf{t}_{N_t} - \mathbf{s}\|}]^T$ is the transmit near-field response vector, $\mathbf{f}_r = [e^{j\frac{2\pi}{\lambda}\|\mathbf{r}_1 - \mathbf{s}\|}, \dots, e^{j\frac{2\pi}{\lambda}\|\mathbf{r}_{N_r} - \mathbf{s}\|}]^T$ is the receive near-field response vector, and ρ_s is the round-trip channel coefficient.

A. System with Linear Precoding

For the system with linear precoding, the transmitted ISAC signal that ensures high-quality communication and sensing functionalities is given by

$$\mathbf{x} = \sum_{k=1}^K \mathbf{W}_k \mathbf{s}_k + \mathbf{v} s_0, \quad (3)$$

where $\mathbf{W}_k \in \mathbb{C}^{N_t \times N_k}$ is the communication precoding matrix for transmission to user k , and $\mathbf{s}_k \in \mathbb{C}^{N_k \times 1}$ is the corresponding transmitted signal, which consists of independent and identically distributed (i.i.d.) symbols that are distributed according to $\mathcal{CN}(0, 1)$. Moreover, $\mathbf{v} \in \mathbb{C}^{N_t \times 1}$ is the sensing transmit beamformer and s_0 is the sensing signal that satisfies $\mathbb{E}\{|s_0|^2\} = 1$.

a) *Communication Model:* For user k , the received signal is given by

$$\mathbf{y}_k = \mathbf{H}_k \mathbf{W}_k \mathbf{s}_k + \mathbf{H}_k \sum_{u=1, u \neq k}^K \mathbf{W}_u \mathbf{s}_u + \mathbf{H}_k \mathbf{v} s_0 + \mathbf{n}_k, \quad (4)$$

where \mathbf{H}_k is given (1) and $\mathbf{n}_k \in \mathbb{C}^{N_k \times 1}$ is the noise vector with i.i.d. elements distributed according to $\mathcal{CN}(0, \sigma_k^2)$, where σ_k^2 is the noise variance at user k .

From (4), the achievable rate for user k is written as

$$R_{L,k} = \ln \left| \mathbf{I} + \mathbf{H}_k \mathbf{W}_k \mathbf{W}_k^H \mathbf{H}_k^H \left(\sum_{u=1, u \neq k}^K \mathbf{H}_k \mathbf{W}_u \mathbf{W}_u^H \mathbf{H}_k^H + \mathbf{H}_k \mathbf{v} \mathbf{v}^H \mathbf{H}_k^H + \sigma_k^2 \mathbf{I}_{N_u} \right)^{-1} \right|. \quad (5)$$

Note that the communication rate in (5) is expressed in nat/s for mathematical convenience.

b) *Sensing Model:* At the receive ULA of the BS, the receive signal is given by

$$\mathbf{y}_B = \mathbf{G} \mathbf{v} s_0 + \mathbf{G} \sum_{u=1}^K \mathbf{W}_u \mathbf{s}_u + \mathbf{z}, \quad (6)$$

where \mathbf{G} is given by (2) and $\mathbf{z} \in \mathbb{C}^{N_r \times 1}$ is the noise vector with i.i.d. elements distributed according to $\mathcal{CN}(0, \sigma_z^2)$.

After implementing the receive signal combiner $\mathbf{u} \in \mathbb{C}^{N_r \times 1}$, the resulting signal is given by

$$y_s = \mathbf{u}^H \mathbf{y}_B = \mathbf{u}^H \mathbf{G} \mathbf{v} s_0 + \mathbf{u}^H \mathbf{G} \sum_{k=1}^K \mathbf{W}_k \mathbf{s}_k + \mathbf{u}^H \mathbf{z}, \quad (7)$$

and the radar sensing capability can be evaluated via the sensing SINR, which is defined as

$$\gamma_s = \frac{P_s}{\mathbf{u}^H \left(\sum_{k=1}^K \mathbf{G} \mathbf{W}_k \mathbf{W}_k^H \mathbf{G}^H + \sigma_z^2 \mathbf{I}_{N_u} \right) \mathbf{u}}, \quad (8)$$

where $P_s = \mathbf{u}^H \mathbf{G} \mathbf{v} \mathbf{v}^H \mathbf{G}^H \mathbf{u}$ is the sensing signal power.

B. System with ZF Precoding

In the case of ZF precoding, the transmitted ISAC signal is given by

$$\mathbf{x} = \mathbf{P}_e \mathbf{s}_e + \mathbf{v} s_0, \quad (9)$$

where $\mathbf{s}_e = [s_1^T, s_2^T, \dots, s_K^T]^T \in \mathbb{C}^{KN_u \times 1}$. The precoding matrix that is defined as

$$\mathbf{P}_e = \beta_e \mathbf{H}_e^H (\mathbf{H}_e \mathbf{H}_e^H)^{-1} \in \mathbb{C}^{N_t \times KN_u},$$

where $\mathbf{H}_e = [\mathbf{H}_1^T, \mathbf{H}_2^T, \dots, \mathbf{H}_K^T]^T \in \mathbb{C}^{KN_u \times N_t}$, and the scaling coefficient that maintains a constant transmit power is equal to

$$\beta_e = \sqrt{\frac{P_{\max}}{\text{Tr}((\mathbf{H}_e \mathbf{H}_e^H)^{-1})}}. \quad (10)$$

a) *Communication Model*: From the previous expressions, a compact representation of the received signal vectors for all users, $\mathbf{y}_e = [\mathbf{y}_1^T, \mathbf{y}_2^T, \dots, \mathbf{y}_K^T]^T$, can be expressed as

$$\mathbf{y}_e = \mathbf{H}_e \mathbf{x} + \mathbf{n}_e = \beta_e \mathbf{H}_e \mathbf{s}_e + \mathbf{H}_e \mathbf{v} s_0 + \mathbf{n}_e, \quad (11)$$

where $\mathbf{n}_e = [\mathbf{n}_1^T, \mathbf{n}_2^T, \dots, \mathbf{n}_K^T]^T$. For user k , the received signal vector is given by

$$\mathbf{y}_k = \beta_e \mathbf{H}_k \mathbf{s}_k + \mathbf{H}_k \mathbf{v} s_0 + \mathbf{n}_k, \quad (12)$$

and the achievable rate for this user can be written as

$$R_{Z,k} = \ln \left| \beta_e^2 \mathbf{I} + \mathbf{H}_k \mathbf{v} \mathbf{v}^H \mathbf{H}_k^H + \sigma_k^2 \mathbf{I}_{N_u} \right| - \ln \left| \mathbf{H}_k \mathbf{v} \mathbf{v}^H \mathbf{H}_k^H + \sigma_k^2 \mathbf{I}_{N_u} \right|. \quad (13)$$

b) *Sensing Model*: The receive signal vector at the receive ULA of the BS is given by

$$\mathbf{y}_B = \mathbf{G} \mathbf{v} s_0 + \mathbf{G} \mathbf{P}_e \mathbf{s}_e + \mathbf{z}. \quad (14)$$

After implementing the receive signal combiner $\mathbf{u} \in \mathbb{C}^{N_r \times 1}$, the resulting signal is written as

$$y_s = \mathbf{u}^H \mathbf{y}_B = \mathbf{u}^H \mathbf{G} \mathbf{v} s_0 + \mathbf{u}^H \mathbf{G} \mathbf{P}_e \mathbf{s}_e + \mathbf{u}^H \mathbf{z}, \quad (15)$$

and the sensing SINR is given as

$$\gamma_s = \frac{P_s}{\mathbf{u}^H (\mathbf{G} \mathbf{P}_e \mathbf{P}_e^H \mathbf{G}^H + \sigma_z^2 \mathbf{I}_{N_u}) \mathbf{u}}, \quad (16)$$

where $P_s = \mathbf{u}^H \mathbf{G} \mathbf{v} \mathbf{v}^H \mathbf{G}^H \mathbf{u}$ is the sensing signal power.

C. Problem Formulation

In this paper, our goal is to maximize the WSR, while at the same time maintaining a minimum SINR performance level of γ_s for target sensing. Therefore, the appropriate optimization problem for the system with linear precoding can be formulated as follows:

$$\underset{\mathbf{u}, \{\mathbf{W}_k\}, \mathbf{v}, \{\mathbf{t}_m\}, \{\mathbf{q}_{k,b}\}}{\text{maximize}} \quad \text{WSR} = \sum_{k=1}^K w_k R_{L,k} \quad (17a)$$

$$\text{s.t.} \quad \text{Tr} \left(\sum_{k=1}^K \mathbf{W}_k \mathbf{W}_k^H \right) \leq P_{\max}, \quad (17b)$$

$$\gamma_s \geq \gamma_0, \quad (17c)$$

$$\|\mathbf{v}\|^2 = 1, \quad (17d)$$

$$\|\mathbf{u}\|^2 = 1, \quad (17e)$$

$$\mathbf{t}_m \in C_t, \forall m, \quad (17f)$$

$$\mathbf{q}_{k,b} \in C_k, \forall k, b, \quad (17g)$$

$$\|\mathbf{t}_{m_1} - \mathbf{t}_{m_2}\| \geq d_{\min}, 1 \leq m_1 \neq m_2 \leq N_t, \quad (17h)$$

$$\|\mathbf{q}_{k,b_1} - \mathbf{q}_{k,b_2}\| \geq d_{\min}, 1 \leq b_1 \neq b_2 \leq N_u, \forall k, \quad (17i)$$

where w_k is the rate weight for user k . It should be noted that constraint (17b) specifies that the total transmit power should not exceed the available transmit power budget P_{\max} . Constraint (17c) specifies that the sensing SINR has to be above the threshold γ_0 . Constraints (17d) and (17e) indicate the unit-energy property of the sensing transmit beamformer and the sensing receive combiner. Constraints (17f) and (17g) specify the moving regions of the transmit and users' MAs, respectively. Constraints (17h) and (17i) ensure the minimum inter-MA distance d_{\min} for the transmit and users' MAs.

Similarly as for linear precoding, the appropriate optimization problem for the system with ZF precoding can be expressed as

$$\underset{\mathbf{u}, \mathbf{v}, \{\mathbf{t}_m\}, \{\mathbf{q}_{k,b}\}}{\text{maximize}} \quad \text{WSR} = \sum_{k=1}^K w_k R_{Z,k} \quad (18a)$$

$$\text{s.t.} \quad \text{Tr}(\mathbf{P}_e \mathbf{P}_e^H) \leq P_{\max}, \quad (18b)$$

$$\gamma_s \geq \gamma_0, \quad (18c)$$

$$\|\mathbf{v}\|^2 = 1, \quad (18d)$$

$$\|\mathbf{u}\|^2 = 1, \quad (18e)$$

$$\mathbf{t}_m \in C_t, \forall m, \quad (18f)$$

$$\mathbf{q}_{k,b} \in C_k, \forall k, b, \quad (18g)$$

$$\|\mathbf{t}_{m_1} - \mathbf{t}_{m_2}\| \geq d_{\min}, 1 \leq m_1 \neq m_2 \leq N_t, \quad (18h)$$

$$\|\mathbf{q}_{k,b_1} - \mathbf{q}_{k,b_2}\| \geq d_{\min}, 1 \leq b_1 \neq b_2 \leq N_u, \forall k. \quad (18i)$$

An important difference between the previous two problems is that the precoding matrices $\{\mathbf{W}_k\}$ are optimization variables in (17), while the precoding matrix \mathbf{P}_e is not considered as an optimization variable in (18). The reason is that $\{\mathbf{W}_k\}$ are independent from other optimization variables in (17). On the other hand, \mathbf{P}_e depends on the users' channel matrices and consequently on the positions of the BS and users' MAs. Therefore, the optimization of the positions of these MAs will implicitly determine \mathbf{P}_e .

III. PROBLEM SOLUTION FOR SYSTEM WITH LINEAR PRECODING

This problem (17) is difficult to solve due to the non-convexity of the objective function, the coupling between the optimization variables, and the unit modulus constraints. To deal with it, we propose an AO-based algorithm which individually optimizes each of the optimization variables separately and is elaborated in more details in the sequel.

A. Optimization of the Sensing Receive Beamformer

Note that the optimal sensing receive beamformer \mathbf{u} has to maximize the sensing SINR γ_s in (8). After reformulating the numerator of γ_s as

$$\mathbf{u}^H \mathbf{G} \mathbf{v} \mathbf{v}^H \mathbf{G}^H \mathbf{u} = (\rho_s^2 \mathbf{f}_t^H \mathbf{v} \mathbf{v}^H \mathbf{f}_t) \times (\mathbf{u}^H \mathbf{f}_r \mathbf{f}_r^H \mathbf{u}), \quad (19)$$

we can observe that $\rho_s^2 \mathbf{f}_t^H \mathbf{v} \mathbf{v}^H \mathbf{f}_t \geq 0$ is independent of \mathbf{u} . Hence, the appropriate optimization problem can be expressed as

$$\begin{aligned} & \underset{\mathbf{u}}{\text{maximize}} \quad \frac{\mathbf{u}^H \mathbf{f}_r \mathbf{f}_r^H \mathbf{u}}{\mathbf{u}^H \mathbf{D}_l \mathbf{u}} \\ & \text{s.t.} \quad (17e), \end{aligned} \quad (20a)$$

where $\mathbf{D}_l = \sum_{u=1}^K \mathbf{G} \mathbf{W}_u \mathbf{W}_u^H \mathbf{G}^H + \sigma_z^2 \mathbf{I}_{N_r}$. From [31], the optimal \mathbf{u} is given by

$$\mathbf{u}^* = \frac{\mathbf{D}_l^{-1} \mathbf{f}_r}{\|\mathbf{D}_l^{-1} \mathbf{f}_r\|}. \quad (21)$$

B. Optimization of the Communication Precoding Matrices

We remark that the objective function in (17a) is neither convex nor concave with respect to the precoding matrices $\{\mathbf{W}_k\}$. To deal with this, we exploit the following inequality to derive a tight concave lower bound on the achievable rate of each user. For matrices \mathbf{X} and $\bar{\mathbf{X}}$ with size $p \times q$, and matrices $\mathbf{Y} \succcurlyeq \mathbf{0}$ and $\bar{\mathbf{Y}} \succcurlyeq \mathbf{0}$ with size $p \times p$, the following inequality is valid [32]:

$$\begin{aligned} & \ln |\mathbf{I} + \mathbf{X}^H \mathbf{Y}^{-1} \mathbf{X}| \geq \ln |\mathbf{I} + \bar{\mathbf{X}}^H \bar{\mathbf{Y}}^{-1} \bar{\mathbf{X}}| \\ & - \text{Tr}\{\bar{\mathbf{X}}^H \bar{\mathbf{Y}}^{-1} \bar{\mathbf{X}}\} + 2\Re\{\text{Tr}\{\bar{\mathbf{X}}^H \bar{\mathbf{Y}}^{-1} \mathbf{X}\}\} \\ & - \text{Tr}\{(\bar{\mathbf{Y}} + \bar{\mathbf{X}} \bar{\mathbf{X}}^H) \bar{\mathbf{X}} \bar{\mathbf{X}}^H \bar{\mathbf{Y}}^{-1} (\mathbf{Y} + \mathbf{X} \mathbf{X}^H)\}, \end{aligned} \quad (22)$$

Let $\{\mathbf{W}_k^{(n)}\}$ denote the value of $\{\mathbf{W}_k\}$ after n iterations, $\mathbf{X} = \mathbf{H}_k \mathbf{W}_k$, $\bar{\mathbf{X}} = \mathbf{H}_k \mathbf{W}_k^{(n)}$, $\mathbf{Y} = \sum_{u=1, u \neq k}^K \mathbf{H}_k \mathbf{W}_u \mathbf{W}_u^H \mathbf{H}_k^H + \mathbf{H}_k \mathbf{v} \mathbf{v}^H \mathbf{H}_k^H + \sigma_k^2 \mathbf{I}_{N_u}$ and $\bar{\mathbf{Y}} = \sum_{u=1, u \neq k}^K \mathbf{H}_k \mathbf{W}_u^{(n)} (\mathbf{W}_u^{(n)})^H \mathbf{H}_k^H + \mathbf{H}_k \mathbf{v} \mathbf{v}^H \mathbf{H}_k^H + \sigma_k^2 \mathbf{I}_{N_u}$. After a few simple mathematical steps, (22) results in

$$\begin{aligned} R_{L,k} & \geq \hat{R}_{L,k} = \ln \left| \mathbf{I} + \mathbf{W}_k^{(n)H} \mathbf{H}_k^H (\mathbf{F}_k^{(n)})^{-1} \mathbf{H}_k \mathbf{W}_k^{(n)} \right| \\ & - \text{Tr}(\mathbf{W}_k^{(n)H} \mathbf{H}_k^H (\mathbf{F}_k^{(n)})^{-1} \mathbf{H}_k \mathbf{W}_k^{(n)}) \\ & + 2\Re(\text{Tr}(\mathbf{W}_k^{(n)H} \mathbf{H}_k^H (\mathbf{F}_k^{(n)})^{-1} \mathbf{H}_k \mathbf{W}_k)) \\ & - \text{Tr}\left(\sum_{u=1}^K \mathbf{W}_u^H \mathbf{H}_k^H \mathbf{A}_k \mathbf{H}_k \mathbf{W}_u\right) \\ & - \text{Tr}(\mathbf{A}_k (\mathbf{H}_k \mathbf{v} \mathbf{v}^H \mathbf{H}_k^H + \sigma_k^2 \mathbf{I}_{N_u})), \end{aligned} \quad (23)$$

where $\mathbf{F}_k^{(n)} = \bar{\mathbf{Y}}$ and $\mathbf{A}_k = (\mathbf{F}_k^{(n)} + \mathbf{H}_k \mathbf{W}_k^{(n)} \mathbf{W}_k^{(n)H} \mathbf{H}_k^H)^{-1} \mathbf{H}_k \mathbf{W}_k^{(n)} \mathbf{W}_k^{(n)H} \mathbf{H}_k^H (\mathbf{F}_k^{(n)})^{-1}$.

Now, it is easy to see that this lower bound is a concave function of $\{\mathbf{W}_k\}$. Furthermore, the constraint (17c) can be reformulated as

$$\kappa_l \triangleq \mathbf{u}^H \mathbf{G} (\gamma_0 \sum_{u=1}^K \mathbf{W}_u \mathbf{W}_u^H - \mathbf{v} \mathbf{v}^H) \mathbf{G}^H \mathbf{u} + \gamma_0 \sigma_z^2 \mathbf{u}^H \mathbf{u} \leq 0. \quad (24)$$

Hence, the precoding matrix optimization problem can be formulated as

$$\underset{\{\mathbf{W}_k\}}{\text{maximize}} \quad \widehat{\text{WSR}} = \sum_{k=1}^K w_k \hat{R}_{L,k} \quad (25a)$$

$$\text{s.t.} \quad \text{Tr}\left(\sum_{k=1}^K \mathbf{W}_k \mathbf{W}_k^H\right) \leq P_{\max}, \quad (25b)$$

(24),

which can be solved by any conventional optimization solver. Finally, the algorithm for optimizing the precoding matrices $\{\mathbf{W}_k\}$ is summarized in Algorithm 1.

Algorithm 1: SCA-based Method for Optimizing the Communication Precoding Matrices

Input: $\{\mathbf{W}_k^{(0)}\}$, $n \leftarrow 0$
1 repeat
 2 Solve (25) to obtain $\{\mathbf{W}_k^{(n+1)}\}$
 3 Calculate $\widehat{\text{WSR}}^{(n+1)}$ according to (25a)
 4 $n \leftarrow n + 1$
 5 **until** $\widehat{\text{WSR}}^{(n)} - \widehat{\text{WSR}}^{(n-1)} < \epsilon_s$
Output: $\{\mathbf{W}_k^*\} = \{\mathbf{W}_k^{(n)}\}$

C. Optimization of the Sensing Transmit Beamformer

Similarly as in the previous subsection, we use the SCA method to find the optimal transmit beamformer \mathbf{v} , but we now introduce the covariance matrix $\mathbf{V} = \mathbf{v} \mathbf{v}^H$. As a result, the achievable rate of user k can be written as

$$\begin{aligned} R_{L,k} & = \ln \left| \sum_{u=1}^K \mathbf{H}_k \mathbf{W}_u \mathbf{W}_u^H \mathbf{H}_k^H + \mathbf{H}_k \mathbf{V} \mathbf{H}_k^H + \sigma_k^2 \mathbf{I}_{N_u} \right| \\ & - \ln \left| \sum_{u=1, u \neq k}^K \mathbf{H}_k \mathbf{W}_u \mathbf{W}_u^H \mathbf{H}_k^H + \mathbf{H}_k \mathbf{V} \mathbf{H}_k^H + \sigma_k^2 \mathbf{I}_{N_u} \right|. \end{aligned} \quad (26)$$

Denoting by $\mathbf{B}_k(\mathbf{V}) = \sum_{u=1, u \neq k}^K \mathbf{H}_k \mathbf{W}_u \mathbf{W}_u^H \mathbf{H}_k^H + \mathbf{H}_k \mathbf{V} \mathbf{H}_k^H + \sigma_k^2 \mathbf{I}_{N_u}$, the first-order Taylor approximation to the second term in (26) is given by

$$\begin{aligned} \ln |\mathbf{B}_k(\mathbf{V})| & \leq \ln |\mathbf{B}_k(\mathbf{V}^{(n)})| \\ & + \text{Tr}(\mathbf{H}_k^H (\mathbf{B}_k(\mathbf{V}^{(n)}))^{-1} \mathbf{H}_k (\mathbf{V} - \mathbf{V}^{(n)})), \end{aligned} \quad (27)$$

where $\mathbf{V}^{(n)}$ is the value of \mathbf{V} after n iterations. Now, (26) can be lower bounded as

$$\begin{aligned} R_{L,k} & \geq \bar{R}_{L,k} = \ln |\mathbf{B}_k(\mathbf{V}) + \mathbf{H}_k \mathbf{W}_k \mathbf{W}_k^H \mathbf{H}_k^H| - \ln |\mathbf{B}_k(\mathbf{V}^{(n)})| \\ & - \text{Tr}(\mathbf{H}_k^H (\mathbf{B}_k(\mathbf{V}^{(n)}))^{-1} \mathbf{H}_k (\mathbf{V} - \mathbf{V}^{(n)})). \end{aligned} \quad (28)$$

From the above, the appropriate optimization problem can be formulated as

$$\underset{\mathbf{V}}{\text{maximize}} \quad \overline{\text{WSR}} = \sum_{k=1}^K w_k \bar{R}_{L,k} \quad (29a)$$

$$\text{s.t.} \quad \text{Tr}(\mathbf{V}) \leq 1, \quad (29b)$$

$$\text{rank}(\mathbf{V}) = 1, \quad (29c)$$

$$(24).$$

We observe that the rank-1 constraint (29c) is not convex. Also, this constraint is equivalent to the maximization of $\beta_{\max}(\mathbf{V}) - \text{Tr}(\mathbf{V})$, where $\beta_{\max}(\mathbf{V})$ is the largest eigenvalue of \mathbf{V} . Exploiting the inequality $\beta_{\max}(\mathbf{V}) \geq \beta_{\max}(\mathbf{V}^{(n)}) + \text{Tr}(\chi^{(n)} \chi^{(n)H} (\mathbf{V} - \mathbf{V}^{(n)}))$, where $\chi^{(n)}$ is the eigenvector corresponding to $\beta_{\max}(\mathbf{V}^{(n)})$, the previous optimization problem can be expressed as

$$\underset{\mathbf{V}}{\text{maximize}} \quad \overline{\text{WSR}} + \zeta \mathcal{M} \quad (30a)$$

$$\text{s.t.} \quad (24), (29b),$$

where $\mathcal{M} = \beta_{\max}(\mathbf{V}^{(n)}) + \text{Tr}(\chi^{(n)} \chi^{(n)H} (\mathbf{V} - \mathbf{V}^{(n)})) - \text{Tr}(\mathbf{V})$, and ζ is the penalty parameter. We notice that this optimization problem is now convex, and can thus be solved by a standard optimization solver. The algorithm for optimizing the transmit sensing beamformer \mathbf{v} is presented in Algorithm 2.

Algorithm 2: SCA-based Method for Optimizing the Sensing Transmit Beamformer

Input: $\mathbf{v}, \zeta, n \leftarrow 0$
 1 $\mathbf{V}^{(0)} = \mathbf{v}\mathbf{v}^H$
 2 **repeat**
 3 Calculate $\beta_{\max}(\mathbf{V}^{(n)})$ and $\chi^{(n)}$
 4 Solve (30) to obtain $\mathbf{V}^{(n+1)}$
 5 Calculate $\overline{\text{WSR}}^{(n+1)}$ according to (29a)
 6 $n \leftarrow n + 1$
 7 **until** $\overline{\text{WSR}}^{(n)} - \overline{\text{WSR}}^{(n-1)} \geq \epsilon_s$
 8 Calculate $\beta_{\max}(\mathbf{V}^{(n)})$ and $\chi^{(n)}$
Output: $\mathbf{v}^* = (\beta_{\max}(\mathbf{V}^{(n)}))^{1/2} \chi^{(n)}$

D. Optimization of MA Positions of User k

The optimization of the MA positions of user k aims to maximize its achievable communication rate, $R_{L,k}$. The appropriate optimization problem can be formulated as

$$\underset{\{\mathbf{q}_{k,b}\}}{\text{maximize}} R_{L,k} \quad (31a)$$

$$\text{s.t. (17g), (17i)}. \quad (31b)$$

To solve this problem, we utilize the PGM approach. If the MA positions of user k after n iterations are denoted by $\mathbf{q}_k^{(n)}$, then the MA positions in the $(n+1)$ -th iteration can be obtained as

$$\mathbf{q}_k^{(n+1)} = P(\mathbf{q}_k^{(n)} + \mu_k^{(n)} \nabla_{\mathbf{q}_k} R_k(\mathbf{q}_k^{(n)})), \quad (32)$$

where $\mu_k^{(n)}$ is the step size. The gradient of R_k with respect to (w.r.t.) \mathbf{q}_k is determined by the gradients of R_k w.r.t. the individual MA coordinates:

$$\nabla_{\mathbf{q}_k} R_{L,k} = [\nabla_{x_{k,1}} R_{L,k}, \nabla_{y_{k,1}} R_{L,k}, 0, \dots, \nabla_{x_{k,N_k}} R_{L,k}, \nabla_{y_{k,N_k}} R_{L,k}, 0]^T.$$

and these gradients are provided in the following lemma.

Lemma 1. *The gradients of R_k w.r.t. the x and y coordinate of the b -th MA of user k are given by (35) and (36) on the next page, where*

$$\mathbf{C}_1 = \mathbf{T}_1 \mathbf{H}_k^H \mathbf{A}_1^{-1}, \quad (33)$$

$$\mathbf{C}_{2,k} = \mathbf{T}_2 \mathbf{H}_k^H \mathbf{A}_{2,k}^{-1}, \quad (34)$$

where $\mathbf{T}_1 = \sum_{u=1}^K \mathbf{W}_u \mathbf{W}_u^H + \mathbf{v}\mathbf{v}^H$, $\mathbf{T}_{2,k} = \mathbf{T}_1 - \mathbf{W}_k \mathbf{W}_k^H$, $\mathbf{A}_1 = \mathbf{H}_k \mathbf{T}_1 \mathbf{H}_k^H + \sigma_k^2 \mathbf{I}_{N_u}$ and $\mathbf{A}_{2,k} = \mathbf{H}_k \mathbf{T}_{2,k} \mathbf{H}_k^H + \sigma_k^2 \mathbf{I}_{N_u}$.

Proof: See Appendix A. ■

The gradient projection is performed element-wise and independently for each MA coordinate. For the x -coordinate of MA b , the gradient projection is given by

$$P(x_{k,b}) = \begin{cases} x_{\max} & x_{\max} < x_{k,b}, \\ x_{k,b} & x_{\min} \leq x_{k,b} \leq x_{\max}, \\ x_{\min} & x_{k,b} < x_{\min}, \end{cases} \quad (37)$$

where $x_{\max} = x_{u,k} + a_k/2$ and $x_{\min} = x_{u,k} - a_k/2$. The projection for y coordinates is done in a similar way. In each iteration, the step size $\mu_k^{(n)}$ is adjusted, i.e., decreased, using the backtracking line search until the constraint (17i) and the ArmijoGoldstein condition

$$R_k(\mathbf{q}_k^{(n+1)}) - R_k(\mathbf{q}_k^{(n)}) \geq \delta \|\mathbf{q}_k^{(n+1)} - \mathbf{q}_k^{(n)}\|^2, \quad (38)$$

where δ is a small positive number, are both satisfied.

E. Optimization of the Transmit MA Positions at the BS

The optimal transmit MA positions at the BS are those that solve the following optimization problem:

$$\underset{\{\mathbf{t}_m\}}{\text{maximize}} \text{WSR} = \sum_{k=1}^K w_k R_{L,k} \quad (39a)$$

$$\text{s.t. (17c), (17f), (17h)}. \quad (39b)$$

Using the equivalent formulation of (17c) in (24) and implementing the ALM [33], we can reformulate the previous optimization problem as

$$\underset{\{\mathbf{t}_m\}}{\text{minimize}} L(\mathbf{t}) = - \sum_{k=1}^K w_k R_{L,k} + \eta \kappa_l + \frac{1}{2} p \kappa_l^2 \quad (40a)$$

$$\text{s.t. (17f), (17h)}, \quad (40b)$$

where $\mathbf{t} = [\mathbf{t}_1^T, \mathbf{t}_2^T, \dots, \mathbf{t}_{N_t}^T]^T$ and η is the Lagrangian multiplier and the penalty factor is given by

$$p = \begin{cases} 0 & \kappa_l \leq 0 \text{ and } \eta = 0, \\ p_0 & \text{otherwise.} \end{cases} \quad (41)$$

To solve (40), we implement the PGM via

$$\mathbf{t}^{(n+1)} = P(\mathbf{t}^{(n)} - \nu^{(n)} \nabla_{\mathbf{t}} L(\mathbf{t}^{(n)})), \quad (42)$$

where $\nu^{(n)}$ is the step size, and the gradient projection is performed similarly as in (37). The gradient $\nabla_{\mathbf{t}} L(\mathbf{t}^{(n)})$ is determined by the gradients of $L(\mathbf{t}^{(n)})$ w.r.t. the coordinates of individual BS transmit MAs. For the m -th BS transmit MA, these gradients are given by

$$\nabla_{x_m} L(\mathbf{t}) = - \sum_{k=1}^K w_k \nabla_{x_m} R_{L,k} + (\eta + p \kappa_l) \nabla_{x_m} \kappa_l, \quad (43)$$

$$\nabla_{y_m} L(\mathbf{t}) = - \sum_{k=1}^K w_k \nabla_{y_m} R_{L,k} + (\eta + p \kappa_l) \nabla_{y_m} \kappa_l, \quad (44)$$

where the gradients of $R_{L,k}$ and κ_l w.r.t. the specified MA coordinates are defined in the following lemma.

Lemma 2. *The gradients of $R_{L,k}$ w.r.t. the coordinates of the m -th BS transmit MA are provided in (45) and (46), shown on the next page.*

Proof: The derivation of the gradients of $R_{L,k}$ w.r.t. to the BS MA coordinates is similar to the derivation of the gradients of R_k w.r.t. to the users' MA coordinates in Appendix A. After substituting

$$\frac{d\mathbf{H}_k(b, m)}{dx_m} = j \frac{2\pi \rho_k}{\lambda} \frac{x_m - x_{k,b}}{\|\mathbf{t}_m - \mathbf{q}_{k,b}\|} e^{j \frac{2\pi}{\lambda} \|\mathbf{t}_m - \mathbf{q}_{k,b}\|}, \quad (47)$$

$$\frac{d\mathbf{H}_k(b, m)}{dy_m} = j \frac{2\pi \rho_k}{\lambda} \frac{y_m - y_{k,b}}{\|\mathbf{t}_m - \mathbf{q}_{k,b}\|} e^{j \frac{2\pi}{\lambda} \|\mathbf{t}_m - \mathbf{q}_{k,b}\|}, \quad (48)$$

into (72) and (73), and a few simple algebraic steps, we obtain (45) and (46). ■

Lemma 3. *The gradients of κ_l w.r.t. the coordinates of the m -th BS transmit MA are given by*

$$\nabla_{x_m} \kappa_l = - \frac{4\pi \rho_s}{\lambda} \mathcal{J} \left(\mathbf{e}(m) e^{j \frac{2\pi}{\lambda} \|\mathbf{t}_m - \mathbf{s}_l\|} \frac{x_m - x_l}{\|\mathbf{t}_m - \mathbf{s}_l\|} \right), \quad (49)$$

$$\nabla_{y_m} \kappa_l = - \frac{4\pi \rho_s}{\lambda} \mathcal{J} \left(\mathbf{e}(m) e^{j \frac{2\pi}{\lambda} \|\mathbf{t}_m - \mathbf{s}_l\|} \frac{y_m - y_l}{\|\mathbf{t}_m - \mathbf{s}_l\|} \right), \quad (50)$$

for $\mathbf{M} = \gamma_0 \sum_{u=1}^K \mathbf{W}_u \mathbf{W}_u^H - \mathbf{v}\mathbf{v}^H$ and $\mathbf{e} = \mathbf{f}_r^H \mathbf{u}\mathbf{u}^H \mathbf{M}\mathbf{G}$.

Proof: See Appendix B. ■

The overall algorithm for optimizing the BS transmit MA positions is outlined in Algorithm 3. In the first part, the MA positions are iteratively optimized using the PGM until the

$$\nabla_{x_{k,b}} R_{L,k} = \frac{4\pi\rho_k}{\lambda} \mathfrak{J} \left(\sum_{m=1}^{N_t} [\mathbf{C}_{2,k}(m,b) - \mathbf{C}_1(m,b)] \frac{x_{k,b} - x_m}{\|\mathbf{t}_m - \mathbf{q}_{k,b}\|} e^{j\frac{2\pi}{\lambda}\|\mathbf{t}_m - \mathbf{q}_{k,b}\|} \right) \quad (35)$$

$$\nabla_{y_{k,b}} R_{L,k} = \frac{4\pi\rho_k}{\lambda} \mathfrak{J} \left(\sum_{m=1}^{N_t} [\mathbf{C}_{2,k}(m,b) - \mathbf{C}_1(m,b)] \frac{y_{k,b} - y_m}{\|\mathbf{t}_m - \mathbf{q}_{k,b}\|} e^{j\frac{2\pi}{\lambda}\|\mathbf{t}_m - \mathbf{q}_{k,b}\|} \right) \quad (36)$$

$$\nabla_{x_m} R_{L,k} = \frac{4\pi\rho_k}{\lambda} \mathfrak{J} \left(\sum_{b=1}^{N_k} [\mathbf{C}_{2,k}(m,b) - \mathbf{C}_{1,k}(m,b)] \frac{x_m - x_k^b}{\|\mathbf{t}_m - \mathbf{q}_k^b\|} e^{j\frac{2\pi}{\lambda}\|\mathbf{t}_m - \mathbf{q}_k^b\|} \right) \quad (45)$$

$$\nabla_{y_m} R_{L,k} = \frac{4\pi\rho_k}{\lambda} \mathfrak{J} \left(\sum_{b=1}^{N_k} [\mathbf{C}_{2,k}(m,b) - \mathbf{C}_{1,k}(m,b)] \frac{y_m - y_k^b}{\|\mathbf{t}_m - \mathbf{q}_k^b\|} e^{j\frac{2\pi}{\lambda}\|\mathbf{t}_m - \mathbf{q}_k^b\|} \right) \quad (46)$$

Algorithm 3: ALM for Optimizing the BS Transmit MA Positions

Input: $\mathbf{t}^{(0)}$, $\eta \leftarrow 0$, p_0 , $\theta > 1$

- 1 $i \leftarrow 0$
- 2 **repeat**
- 3 Compute $L(\mathbf{t})$ according to (40a)
- 4 **repeat**
- 5 $n \leftarrow 0$
- 6 **repeat**
- 7 $\mathbf{t}^{(n+1)} = P(\mathbf{t}^{(n)} - \nu^{(n)} \nabla_{\mathbf{t}} L(\mathbf{t}^{(n)}))$
- 8 **if** $L(\mathbf{t}^{(n)}) - L(\mathbf{t}^{(n+1)}) < \delta \|\mathbf{t}^{(n+1)} - \mathbf{t}^{(n)}\|^2$ **or**
- 9 $\|\mathbf{t}_{m_1}^{(n+1)} - \mathbf{t}_{m_2}^{(n+1)}\| < d_{\min}$ (for any $m_1 \neq m_2$) **then**
- 10 $\nu^{(n)} \leftarrow \tau \nu^{(n)}$
- 11 **end**
- 12 **until** $L(\mathbf{t}^{(n)}) - L(\mathbf{t}^{(n+1)}) \geq \delta \|\mathbf{t}^{(n+1)} - \mathbf{t}^{(n)}\|^2$ **and**
- 13 $\|\mathbf{t}_{m_1}^{(n+1)} - \mathbf{t}_{m_2}^{(n+1)}\| \geq d_{\min}$ (for all $m_1 \neq m_2$)
- 14 $n \leftarrow n + 1$
- 15 **until** $\left| \frac{L(\mathbf{t}^{(n)}) - L(\mathbf{t}^{(n-1)})}{L(\mathbf{t}^{(n)})} \right| < \epsilon_L$
- 16 $\mathbf{t}_c^{(i+1)} = \mathbf{t}^{(n)}$
- 17 $\mathbf{t}^{(0)} = \mathbf{t}^{(n)}$
- 18 $\eta = \max(0, \eta + p_0 \kappa_i)$
- 19 $p_0 = \theta p_0$
- 20 $i \leftarrow i + 1$
- 21 **until** $|\text{WSR}(\mathbf{t}_c^{(i)}) - \text{WSR}(\mathbf{t}_c^{(i-1)})| < \epsilon_f$

Output: $\mathbf{t}^* = \mathbf{t}_c^{(i)}$

convergence¹ of $L(\mathbf{t})$, and these MA positions are saved as \mathbf{t}_c . Afterwards, the Lagrangian multiplier η is recomputed and the parameter p_0 , that determines the value of the penalty factor p , is scaled by the constant θ . These steps are repeated until the convergence of the WSR, i.e., until the difference between the WSRs calculated for the MA positions determined by $\mathbf{t}_c^{(i-1)}$ and $\mathbf{t}_c^{(i)}$ is less than the specified threshold.

F. Overall Algorithm

The overall algorithm for solving the problem (17) is summarized in Algorithm 4. Regarding the convergence of Algorithm 4, we first observe that the optimization \mathbf{u} does not change the WSR. Moreover, $\{\mathbf{W}_k\}$ and \mathbf{v} are optimized by using the concave lower bounds of the objective function and implementing convex optimization. Therefore, the appropriate objective values have to satisfy

$$\text{WSR}(\mathbf{u}^{(n+1)}, \{\mathbf{W}_k^{(n)}\}, \mathbf{v}^{(n)}, \{\mathbf{q}_k^{(n)}\})$$

¹It should be noted that this convergence criterion for $L(\mathbf{t})$ is based on the relative change and not on the absolute change between two of its consecutive values. The reason is that $L(\mathbf{t})$ can change by more than an order of magnitude during the optimization process, primarily because of the change of the parameter p_0 (line 17 in Algorithm 3).

Algorithm 4: Overall Optimization Algorithm for Solving (17)

Input: $\mathbf{u}^{(0)}$, $\{\mathbf{W}_k^{(0)}\}$, $\mathbf{v}^{(0)}$, $\{\mathbf{q}_k^{(0)}\}$, $\mathbf{t}^{(0)}$, $\{\rho_k\}$, ρ_s , $\{\mu_k^{(0)}\}$, d_{\min} , $\eta \leftarrow 0$, $\tau \in (0, 1)$, $\delta > 0$, $n \leftarrow 0$

- 1 **repeat**
- 2 Obtain $\mathbf{u}^{(n+1)}$ from (21)
- 3 Obtain $\{\mathbf{W}_k^{(n+1)}\}$ by Algorithm 1
- 4 Obtain $\mathbf{v}^{(n+1)}$ by Algorithm 2
- 5 **for** $k = 1$ to K **do**
- 6 **repeat**
- 7 $\mathbf{q}_k^{(n+1)} = P(\mathbf{q}_k^{(n)} + \mu^{(n)} \nabla_{\mathbf{q}_k} R_k)$
- 8 **if** $R_k(\mathbf{q}_k^{(n+1)}) - R_k(\mathbf{q}_k^{(n)}) < \delta \|\mathbf{q}_k^{(n+1)} - \mathbf{q}_k^{(n)}\|^2$
- 9 **or** $\|\mathbf{q}_{k,b_1}^{(n+1)} - \mathbf{q}_{k,b_2}^{(n+1)}\| < d_{\min}$ (for any $b_1 \neq b_2$) **then**
- 10 $\mu_k^{(n)} \leftarrow \tau \mu_k^{(n)}$
- 11 **end**
- 12 **until** $R_{L,k}(\mathbf{q}_k^{(n+1)}) - R_{L,k}(\mathbf{q}_k^{(n)}) \geq \delta \|\mathbf{q}_k^{(n+1)} - \mathbf{q}_k^{(n)}\|^2$
- 13 **and** $\|\mathbf{q}_{k,b_1}^{(n+1)} - \mathbf{q}_{k,b_2}^{(n+1)}\| \geq d_{\min}$ (for all $b_1 \neq b_2$)
- 14 **end**
- 15 Obtain $\mathbf{t}^{(n+1)}$ by Algorithm 3
- 16 $n \leftarrow n + 1$
- 17 **until** convergence of WSR in (17a)

Output: \mathbf{u}^{opt} , $\{\mathbf{W}_k^{\text{opt}}\}$, \mathbf{v}^{opt} , $\{\mathbf{q}_k^{\text{opt}}\}$

$$\begin{aligned} &\leq \text{WSR}(\mathbf{u}^{(n+1)}, \{\mathbf{W}_k^{(n+1)}\}, \mathbf{v}^{(n)}, \{\mathbf{q}_k^{(n)}\}) \\ &\leq \text{WSR}(\mathbf{u}^{(n+1)}, \{\mathbf{W}_k^{(n+1)}\}, \mathbf{v}^{(n+1)}, \{\mathbf{q}_k^{(n)}\}). \end{aligned} \quad (51)$$

The MA positions of users are optimized by the PGM, which always yields an improved objective value. The same is true for the ALM which adjusts the BS transmit MA positions. From the above we conclude that the objective function is monotonically non-decreasing in each iteration of Algorithm 4. Also, the objective function is upper bounded due to limited communication resources. These two facts guarantee the convergence of the objective function to a stationary point.

IV. PROBLEM SOLUTION FOR SYSTEM WITH ZF PRECODING

Similar to the case of linear precoding, the optimization problem (18) for ZF precoding is also non-convex. For this reason, we propose an AO-based algorithm which individually optimizes each of the optimization variables separately and is elaborated in more detail in the following subsections.

A. Optimization of the Sensing Receive Combiner

Note that the SINR expression (8) for the case of linear precoding is quite similar to the SINR expression (16) for the

case of ZF precoding. Therefore, it easy to see that the optimal receive beamformer can be obtained as

$$\mathbf{u}^* = \frac{\mathbf{D}_z^{-1} \mathbf{f}_r}{\|\mathbf{D}_z^{-1} \mathbf{f}_r\|}, \quad (52)$$

where $\mathbf{D}_z = \mathbf{G} \mathbf{P}_e \mathbf{P}_e^H \mathbf{G}^H + \sigma_z^2 \mathbf{I}_{N_r}$.

B. Optimization of the Sensing Transmit Beamformer

Similarly as for linear precoding, the sensing transmit beamformer is optimized using the SCA method. Using the covariance matrix $\mathbf{V} = \mathbf{v} \mathbf{v}^H$ and the first-order Taylor approximation

$$\ln |\mathbf{E}_k(\mathbf{V})| \leq \ln |\mathbf{E}_k(\mathbf{V}^{(n)})| + \text{Tr}(\mathbf{H}_k^H (\mathbf{E}_k(\mathbf{V}^{(n)}))^{-1} \mathbf{H}_k (\mathbf{V} - \mathbf{V}^{(n)})), \quad (53)$$

where $\mathbf{E}_k(\mathbf{V}) = \mathbf{H}_k \mathbf{V} \mathbf{H}_k^H + \sigma_k^2 \mathbf{I}_{N_u}$, $\mathbf{E}_k(\mathbf{V}^{(n)}) = \mathbf{H}_k \mathbf{V}^{(n)} \mathbf{H}_k^H + \sigma_k^2 \mathbf{I}_{N_u}$ and $\mathbf{V}^{(n)}$ denotes \mathbf{V} after n iterations, the achievable rate of user k can be lower-bounded as

$$R_{Z,k} \geq \tilde{R}_{Z,k} = \ln \left| \beta_e^2 \mathbf{I} + \mathbf{E}_k(\mathbf{V}) \right| - \ln \left| \mathbf{E}_k(\mathbf{V}^{(n)}) \right| - \text{Tr}(\mathbf{H}_k^H (\mathbf{E}_k(\mathbf{V}^{(n)}))^{-1} \mathbf{H}_k (\mathbf{V} - \mathbf{V}^{(n)})).$$

Following the same steps as in the case of linear precoding, the appropriate optimization problem can be formulated as

$$\underset{\mathbf{V}}{\text{maximize}} \sum_{k=1}^K w_k \tilde{R}_{Z,k} + \zeta \mathcal{M} \quad (54a)$$

$$\text{s.t. } \text{Tr}(\mathbf{V}) \leq 1, \quad (54b)$$

$$(18c),$$

where $\mathcal{M} = \beta_{\max}(\mathbf{V}^{(n)}) + \text{Tr}(\chi^{(n)} \chi^{(n)H} (\mathbf{V} - \mathbf{V}^{(n)})) - \text{Tr}(\mathbf{V})$ and ζ is the penalty parameter. Since this problem is convex, it can be solved by any conventional optimization solver, and the appropriate optimization algorithm has the same form as Algorithm 2.

C. Optimization of MA Positions of User k

Changing the MA positions of a single user in a system with ZF precoding affects the achievable rate of all users, as well as the sensing SINR. This is a major difference compared to systems with linear precoding, where any change the MA positions of a user influences only its the achievable rate. Therefore, the optimal MA positions of user k in the considered system with ZF precoding are determined by the following optimization problem:

$$\underset{\{\mathbf{q}_{k,b}\}}{\text{maximize}} \text{WSR} = \sum_{k=1}^K w_k R_{Z,k} \quad (55a)$$

$$\text{s.t. } (18b), (18c), (18g), (18i). \quad (55b)$$

For convenience, the SINR constraint (18c) can be reformulated as

$$\kappa_z \triangleq \mathbf{u}^H \mathbf{G} (\gamma_0 \mathbf{P}_e \mathbf{P}_e^H - \mathbf{v} \mathbf{v}^H) \mathbf{G}^H \mathbf{u} + \gamma_0 \sigma_z^2 \mathbf{u}^H \mathbf{u} \leq 0. \quad (56)$$

To deal with this, similarly as in subsection III-E, we use the ALM and reformulate (55) according to

$$\underset{\{\mathbf{q}_{k,b}\}}{\text{minimize}} L(\mathbf{q}_k) = - \sum_{k=1}^K w_k R_{Z,k} + \eta \kappa_z + \frac{1}{2} p \kappa_z^2 \quad (57a)$$

$$\text{s.t. } (18b), (18g), (18i), \quad (57b)$$

where η is the Lagrangian multiplier and the penalty factor is given by

$$p = \begin{cases} 0 & \kappa_z \leq 0 \text{ and } \eta = 0, \\ p_0 & \text{otherwise.} \end{cases} \quad (58)$$

We employ the PGM to solve (57) via

$$\mathbf{q}_k^{(n+1)} = P(\mathbf{q}_k^{(n+1)} - \alpha^{(n)} \nabla_{\mathbf{q}_k} L(\mathbf{q}_k^{(n)})), \quad (59)$$

where $\alpha^{(n)}$ is the step size. The gradient $\nabla_{\mathbf{q}_k} L(\mathbf{q}_k^{(n)})$ is determined by the gradients of $L(\mathbf{q}_k^{(n)})$ w.r.t. the coordinates of individual MAs of user k . For the b -th ($b \in \{1, \dots, N_k\}$) MA of user k , these gradients are given by

$$\nabla_{x_{k,b}} L(\mathbf{q}_k^{(n)}) = - \sum_{k=1}^K w_k \nabla_{x_{k,b}} R_{Z,u} + (\eta + p) \nabla_{x_{k,b}} \kappa_z, \quad (60)$$

$$\nabla_{y_{k,b}} L(\mathbf{q}_k^{(n)}) = - \sum_{k=1}^K w_k \nabla_{y_{k,b}} R_{Z,u} + (\eta + p) \nabla_{y_{k,b}} \kappa_z, \quad (61)$$

where expressions for the gradients of $R_{Z,u}$ and κ_z w.r.t. the specified MA coordinates are given in the following lemmas.

Lemma 4. The gradients of $R_{Z,u}$ ($u \in \{1, \dots, K\}$) w.r.t. the coordinates of the b -th MA of user k are given by (62) and (63) on the next page, where $\delta_{k,u}$ is the Kronecker delta defined as

$$\delta_{k,u} = \begin{cases} 1 & k = u, \\ 0 & k \neq u, \end{cases}$$

$b_k = (k-1)N_k + b$, $T = \text{Tr}((\mathbf{H}_e \mathbf{H}_e^H)^{-1})$, $\mathbf{B}_e = \mathbf{H}_e^H (\mathbf{H}_e \mathbf{H}_e^H)^{-2}$, $\mathbf{E}_k = \mathbf{H}_k \mathbf{v} \mathbf{v}^H \mathbf{H}_k^H + \sigma_k^2 \mathbf{I}_{N_k}$, $\mathbf{F}_k = \beta_e^2 \mathbf{I}_{N_k} + \mathbf{H}_k \mathbf{v} \mathbf{v}^H \mathbf{H}_k^H + \sigma_k^2 \mathbf{I}_{N_k}$, $\mathbf{F}_u = \beta_e^2 \mathbf{I} + \mathbf{H}_u \mathbf{v} \mathbf{v}^H \mathbf{H}_u^H + \sigma_k^2 \mathbf{I}_{N_u}$ and $\mathbf{G}_k = \mathbf{v} \mathbf{v}^H \mathbf{H}_k^H (\mathbf{F}_k^{-1} - \mathbf{E}_k^{-1})$.

Proof: See Appendix C. ■

Lemma 5. The gradients of κ_z w.r.t. the coordinates of the b -th MA of user k are given by (64) and (65) on the next page, where $b_k = (k-1)N_k + b$, $T = \text{Tr}((\mathbf{H}_e \mathbf{H}_e^H)^{-1})$, $\mathbf{B}_e = \mathbf{H}_e^H (\mathbf{H}_e \mathbf{H}_e^H)^{-2}$, $\mathbf{P}_1 = \mathbf{H}_e^H (\mathbf{H}_e \mathbf{H}_e^H)^{-1}$, $\mathbf{D} = \mathbf{P}_1^H \mathbf{G}^H \mathbf{u} \mathbf{u}^H \mathbf{G}$, $\mathbf{D}_1 = \mathbf{H}_e^H \mathbf{D} \mathbf{H}_e^H (\mathbf{H}_e \mathbf{H}_e^H)^{-2}$ and $\mathbf{D}_2 = (\mathbf{H}_e \mathbf{H}_e^H)^{-1} \mathbf{D} - \mathbf{D} \mathbf{H}_e^H (\mathbf{H}_e \mathbf{H}_e^H)^{-2} \mathbf{H}_e$.

Proof: See Appendix D. ■

The algorithm for optimizing the MA positions of user k is outlined in Algorithm 5 and is very similar to Algorithm 3. One should note that, due to ZF precoding, any change in the coordinates of the MAs of user k requires re-computation of the appropriate channel matrix \mathbf{H}_k as well as the precoding matrix \mathbf{P}_e . On the other hand, only \mathbf{H}_k needs to be recomputed in the case of linear precoding.

D. Optimization of the BS Transmit MA Positions

The optimal BS transmit MA positions are determined by solving the following problem:

$$\underset{\{\mathbf{t}_m\}}{\text{maximize}} \text{WSR} = \sum_{k=1}^K w_k R_{Z,k} \quad (66a)$$

$$\text{s.t. } (18b), (18f), (18h), (56). \quad (66b)$$

This problem can be solved using same optimization method and the same steps as in the previous subsection. The only difference is in the gradients of the WSR and the sensing SINR κ_z w.r.t. the transmit MA coordinates, which are specified in the following lemmas.

Lemma 6. The gradients of $R_{Z,u}$ ($u \in \{1, \dots, K\}$) w.r.t. the coordinates of the m -th BS transmit MA are given by (67) and (68) on the next page, where $\mathbf{E}_u = \mathbf{H}_u \mathbf{v} \mathbf{v}^H \mathbf{H}_u^H + \sigma_u^2 \mathbf{I}_{N_u}$, $\mathbf{F}_u = \beta_e^2 \mathbf{I}_{N_u} + \mathbf{H}_u \mathbf{v} \mathbf{v}^H \mathbf{H}_u^H + \sigma_k^2 \mathbf{I}_{N_u}$ and $\mathbf{G}_u = \mathbf{v} \mathbf{v}^H \mathbf{H}_u^H (\mathbf{F}_u^{-1} - \mathbf{E}_u^{-1})$.

$$\nabla_{x_{k,b}} R_{Z,u} = -\frac{4\pi\rho_k}{\lambda} \mathfrak{J} \left(\sum_{m=1}^{N_t} [P_{\max} T^{-2} \text{Tr}(\mathbf{F}_u^{-1}) \mathbf{B}_e(m, b_r) + \delta_{k,u} \mathbf{G}_k(m, b)] e^{j\frac{2\pi}{\lambda} \|\mathbf{t}_m - \mathbf{q}_{k,b}\|} \frac{x_{k,b} - x_m}{\|\mathbf{t}_m - \mathbf{q}_{k,b}\|} \right) \quad (62)$$

$$\nabla_{y_{k,b}} R_{Z,u} = -\frac{4\pi\rho_k}{\lambda} \mathfrak{J} \left(\sum_{m=1}^{N_t} [P_{\max} T^{-2} \text{Tr}(\mathbf{F}_u^{-1}) \mathbf{B}_e(m, b_r) + \delta_{k,u} \mathbf{G}_k(m, b)] e^{j\frac{2\pi}{\lambda} \|\mathbf{t}_m - \mathbf{q}_{k,b}\|} \frac{y_{k,b} - y_m}{\|\mathbf{t}_m - \mathbf{q}_{k,b}\|} \right) \quad (63)$$

$$\begin{aligned} \nabla_{x_{k,b}} \kappa_z &= -\gamma_0 \mathbf{u}^H \mathbf{G} \mathbf{P}_1 \mathbf{P}_1^H \mathbf{G}^H \mathbf{u} \frac{4\pi\rho_k}{\lambda} P_{\max} T^{-2} \mathfrak{J} \left(\sum_{m=1}^{N_t} \mathbf{B}_e(m, b_r) e^{j\frac{2\pi}{\lambda} \|\mathbf{t}_m - \mathbf{q}_{k,b}\|} \frac{x_{k,b} - x_m}{\|\mathbf{t}_m - \mathbf{q}_{k,b}\|} \right) \\ &\quad + \gamma_0 \beta_e^2 \frac{4\pi\rho_k}{\lambda} \mathfrak{J} \left(\sum_{m=1}^{N_t} \left[\mathbf{D}_1(m, b_r) e^{j\frac{2\pi}{\lambda} \|\mathbf{t}_m - \mathbf{q}_{k,b}\|} + \mathbf{D}_2^T(m, b_r) e^{-j\frac{2\pi}{\lambda} \|\mathbf{t}_m - \mathbf{q}_{k,b}\|} \right] \frac{x_{k,b} - x_m}{\|\mathbf{t}_m - \mathbf{q}_{k,b}\|} \right) \end{aligned} \quad (64)$$

$$\begin{aligned} \nabla_{y_{k,b}} x_m &= -\gamma_0 \mathbf{u}^H \mathbf{G} \mathbf{P}_1 \mathbf{P}_1^H \mathbf{G}^H \mathbf{u} \frac{4\pi\rho_k}{\lambda} P_{\max} T^{-2} \mathfrak{J} \left(\sum_{m=1}^{N_t} \mathbf{B}_e(m, b_r) e^{j\frac{2\pi}{\lambda} \|\mathbf{t}_m - \mathbf{q}_{k,b}\|} \frac{y_{k,b} - y_m}{\|\mathbf{t}_m - \mathbf{q}_{k,b}\|} \right) \\ &\quad + \gamma_0 \beta_e^2 \frac{4\pi\rho_k}{\lambda} \mathfrak{J} \left(\sum_{m=1}^{N_t} \left[\mathbf{D}_1(m, b_r) e^{j\frac{2\pi}{\lambda} \|\mathbf{t}_m - \mathbf{q}_{k,b}\|} + \mathbf{D}_2^T(m, b_r) e^{-j\frac{2\pi}{\lambda} \|\mathbf{t}_m - \mathbf{q}_{k,b}\|} \right] \frac{y_{k,b} - y_m}{\|\mathbf{t}_m - \mathbf{q}_{k,b}\|} \right) \end{aligned} \quad (65)$$

$$\begin{aligned} \nabla_{x_m} R_{Z,u} &= -\frac{4\pi}{\lambda} \mathfrak{J} \left(P_{\max} T^{-2} \text{Tr}(\mathbf{F}_u^{-1}) \sum_{k=1}^K \sum_{b=1}^{N_u} \rho_k \mathbf{B}_e(m, b_r) e^{j\frac{2\pi}{\lambda} \|\mathbf{t}_m - \mathbf{q}_{k,b}\|} \frac{x_m - x_{k,b}}{\|\mathbf{t}_m - \mathbf{q}_{k,b}\|} \right) \\ &\quad - \frac{4\pi\rho_u}{\lambda} \mathfrak{J} \left(\sum_{b=1}^{N_u} \mathbf{G}_u(m, b) e^{j\frac{2\pi}{\lambda} \|\mathbf{t}_m - \mathbf{q}_{u,b}\|} \frac{x_m - x_{u,b}}{\|\mathbf{t}_m - \mathbf{q}_{u,b}\|} \right) \end{aligned} \quad (67)$$

$$\begin{aligned} \nabla_{y_m} R_{Z,u} &= -\frac{4\pi}{\lambda} \mathfrak{J} \left(P_{\max} T^{-2} \text{Tr}(\mathbf{F}_u^{-1}) \sum_{k=1}^K \sum_{b=1}^{N_u} \rho_k \mathbf{B}_e(m, b_r) e^{j\frac{2\pi}{\lambda} \|\mathbf{t}_m - \mathbf{q}_{k,b}\|} \frac{y_m - y_{k,b}}{\|\mathbf{t}_m - \mathbf{q}_{k,b}\|} \right) \\ &\quad - \frac{4\pi\rho_u}{\lambda} \mathfrak{J} \left(\sum_{b=1}^{N_u} \mathbf{G}_u(m, b) e^{j\frac{2\pi}{\lambda} \|\mathbf{t}_m - \mathbf{q}_{u,b}\|} \frac{y_m - y_{u,b}}{\|\mathbf{t}_m - \mathbf{q}_{u,b}\|} \right) \end{aligned} \quad (68)$$

Algorithm 5: ALM for Optimizing the MA Positions of User k

Input: $\mathbf{q}_k^{(0)}$, $\eta \leftarrow 0$, p_0 , θ

- 1 $i \leftarrow 0$
- 2 **repeat**
- 3 Calculate $L(\mathbf{t})$ according to (40a)
- 4 **repeat**
- 5 $n \leftarrow 0$
- 6 **repeat**
- 7 $\mathbf{t}^{(n+1)} = P(\mathbf{t}^{(n)} - \alpha^{(n)} \nabla_{\mathbf{t}} L(\mathbf{t}^{(n)}))$
- 8 **if** $L(\mathbf{q}_k^{(n)}) - L(\mathbf{q}_k^{(n+1)}) < \delta \|\mathbf{q}_k^{(n+1)} - \mathbf{q}_k^{(n)}\|^2$ **or**
- 9 $\|\mathbf{q}_{k,b_1}^{(n+1)} - \mathbf{q}_{k,b_2}^{(n+1)}\| < d_{\min}$ (for any $b_1 \neq b_2$) **then**
- 10 $\alpha^{(n)} \leftarrow \tau \alpha^{(n)}$
- 11 **end**
- 12 **until** $L(\mathbf{q}_k^{(n)}) - L(\mathbf{q}_k^{(n+1)}) \geq \delta \|\mathbf{q}_k^{(n+1)} - \mathbf{q}_k^{(n)}\|^2$ **and**
- 13 $\|\mathbf{q}_{k,b_1}^{(n+1)} - \mathbf{q}_{k,b_2}^{(n+1)}\| \geq d_{\min}$ (for all $b_1 \neq b_2$)
- 14 $n \leftarrow n + 1$
- 15 **until** $\left| \frac{L(\mathbf{q}_k^{(n)}) - L(\mathbf{q}_k^{(n-1)})}{L(\mathbf{q}_k^{(n)})} \right| < \epsilon_L$
- 16 $\mathbf{q}_c^{(i)} = \mathbf{q}_k^{(n)}$
- 17 $\mathbf{q}_k^{(0)} = \mathbf{q}_k^{(n)}$
- 18 $\eta = \max(0, \eta + p_0 \kappa_z)$
- 19 $p_0 = \theta p_0$
- 20 $i \leftarrow i + 1$
- 21 **until** $|\text{WSR}(\mathbf{q}_c^{(i)}) - \text{WSR}(\mathbf{q}_c^{(i-1)})| < \epsilon_f$

Output: $\mathbf{q}_k^* = \mathbf{q}_c^{(i)}$

Proof: The proof is similar to the proof of Lemma 4. ■

Lemma 7. The gradients of κ_z w.r.t. the coordinates of the m -th BS transmit MA are given by (69) and (70) on the next page.

Proof: The proof is similar to the proof of Lemma 5. ■

E. Overall Algorithm

Due to the limited space and similarity with Algorithm 4, we provide only a description of the overall algorithm. In each iteration, the sensing receive combiner is obtained by using (52), which provides a closed-form solution. The sensing transmit beamformer is optimized by the SCA method for which we use a concave lower bound on the user's achievable rate; therefore, it improves the WSR of the system. Also, the MA positions are optimized separately for each user with the ALM, presented in Algorithm 5, which provably increases the WSR. Using the same optimization method, the positions of the BS transmit MAs are adjusted. Hence, we can conclude that the overall algorithm monotonically increases the WSR in each iteration. Also, due to limited communication resources, the WSR must be upper bounded. These two facts guarantee the convergence of the objective function to a stationary point.

Finally, note that full details regarding the computational complexity of the proposed algorithms are omitted due to space considerations.

V. SIMULATION RESULTS

In this section, we evaluate the WSR of the considered schemes with linear precoding (denoted as LP-MA) and ZF precoding (denoted as ZF-MA) by means of Monte Carlo simulations. As benchmarks, we consider schemes that differ from the proposed ones in that the BS transmitter and users have fixed antennas; these are referred to as the LP-FIX and ZF-FIX scheme, respectively. The initial positions of the users' MAs and the BS transmit MAs are the same for all four schemes and are randomly chosen inside the MA regions C_k and C_t , respectively. The free space path loss between the BS and user k is modeled as $\rho_k = \lambda^2 / (4\pi d_{tk})^2$ [26], where $d_{tk} = \|\mathbf{o}_t - \mathbf{o}_k\|$ is the

$$\begin{aligned} \nabla_{x_m} \kappa_z &= -\frac{4\pi\rho_s}{\lambda} \mathfrak{J} \left(\mathbf{e}(m) e^{j\frac{2\pi}{\lambda} \|\mathbf{t}_m - \mathbf{s}_l\|} \frac{x_m - x_s}{\|\mathbf{t}_m - \mathbf{s}_l\|} \right) \\ &\quad - \frac{4\pi}{\lambda} P_{\max} T^{-2} \gamma_0 \mathbf{u}^H \mathbf{G} \mathbf{P}_1 \mathbf{P}_1^H \mathbf{G}^H \mathbf{u} \mathfrak{J} \left(\sum_{k=1}^K \sum_{b=1}^{N_u} \rho_k \mathbf{B}_e(m, b_r) e^{j\frac{2\pi}{\lambda} \|\mathbf{t}_m - \mathbf{q}_{k,b}\|} \frac{x_m - x_{k,b}}{\|\mathbf{t}_m - \mathbf{q}_{k,b}\|} \right) \\ &\quad + \frac{4\pi}{\lambda} \gamma_0 \beta^2 \mathfrak{J} \left(\sum_{k=1}^K \sum_{b=1}^{N_u} \rho_k \left[\mathbf{D}_1(m, b_r) e^{j\frac{2\pi}{\lambda} \|\mathbf{t}_m - \mathbf{q}_{k,b}\|} + \mathbf{D}_2^T(m, b_r) e^{-j\frac{2\pi}{\lambda} \|\mathbf{t}_m - \mathbf{q}_{k,b}\|} \right] \frac{x_m - x_{k,b}}{\|\mathbf{t}_m - \mathbf{q}_{k,b}\|} \right) \end{aligned} \quad (69)$$

$$\begin{aligned} \nabla_{y_m} \kappa_z &= -\frac{4\pi\rho_s}{\lambda} \mathfrak{J} \left(\mathbf{e}(m) e^{j\frac{2\pi}{\lambda} \|\mathbf{t}_m - \mathbf{s}_l\|} \frac{y_m - y_s}{\|\mathbf{t}_m - \mathbf{s}_l\|} \right) \\ &\quad - \frac{4\pi}{\lambda} P_{\max} T^{-2} \gamma_0 \mathbf{u}^H \mathbf{G} \mathbf{P}_1 \mathbf{P}_1^H \mathbf{G}^H \mathbf{u} \mathfrak{J} \left(\sum_{k=1}^K \sum_{b=1}^{N_u} \rho_k \mathbf{B}_e(m, b_r) e^{j\frac{2\pi}{\lambda} \|\mathbf{t}_m - \mathbf{q}_{k,b}\|} \frac{y_m - y_{k,b}}{\|\mathbf{t}_m - \mathbf{q}_{k,b}\|} \right) \\ &\quad + \frac{4\pi}{\lambda} \gamma_0 \beta^2 \mathfrak{J} \left(\sum_{k=1}^K \sum_{b=1}^{N_u} \rho_k \left[\mathbf{D}_1(m, b_r) e^{j\frac{2\pi}{\lambda} \|\mathbf{t}_m - \mathbf{q}_{k,b}\|} + \mathbf{D}_2^T(m, b_r) e^{-j\frac{2\pi}{\lambda} \|\mathbf{t}_m - \mathbf{q}_{k,b}\|} \right] \frac{y_m - y_{k,b}}{\|\mathbf{t}_m - \mathbf{q}_{k,b}\|} \right) \end{aligned} \quad (70)$$

distance between the BS transmit MA array and user k . The round-trip channel coefficient for target sensing is given by $\rho_s = \lambda^2 / ((4\pi)^3 R_t^2 R_r^2)$ [34], where $R_t = \|\mathbf{o}_t - \mathbf{s}\|$ is the distance between the BS transmit MA array and the target, and $R_r = \|\mathbf{o}_r - \mathbf{s}\|$ is the distance between the BS receive antenna array and the target.

In the following simulation setup, the parameters are $f = 30$ GHz (i.e., $\lambda = 1$ cm), $N_t = 16$, $N_r = 8$, $K = 2$, $N_u = 4$, $P_{\max} = 1$ W, $d_{\min} = \lambda/2 = 0.5$ cm, $\gamma_0 = 0.01$, $\zeta = 1$ and $\sigma_k^2 = \sigma_z^2 = -100$ dB. The center of the BS transmit MA region is located $\mathbf{o}_t = [-3 \text{ m}, 10 \text{ m}, 0]^T$ and the length of its side is $L_t = 1$ m. The midpoint of the receive BS ULAs is located at $\mathbf{o}_r = [3 \text{ m}, 10 \text{ m}, 0]^T$ and the length of this ULA is $L_r = 1$ m. Both users are placed at the same distance from the BS transmit MA array in the directions of $\pm\pi/4$ in the xz -plane. The centers of the users' MA regions are located at $\mathbf{o}_{u,1} = [-3 \text{ m} + d_{tk} \sin(-\pi/4), 1.5 \text{ m}, d_{tk} \cos(-\pi/4)]^T$ and $\mathbf{o}_{u,2} = [-3 \text{ m} + d_{tk} \sin(\pi/4), 1.5 \text{ m}, d_{tk} \cos(\pi/4)]^T$, where $d_{tk} = 30$ m, and the side length of each of these regions is $a_k = 15$ cm. The initial positions of the users' antennas are randomly selected inside the specified MA regions. The point target is located at $\mathbf{s} = [10 \text{ m}, 1.5 \text{ m}, 10 \text{ m}]^T$. The CVX tool is used to solve (25), (30) and (54). In the line search procedure for the PGM, all step sizes are initially set to 1, $\delta = 10^{-2}$ and $\tau = 1/2$. The parameters of the ALM are initialized as $\eta = 0$, $p_0 = 1$, $\theta = 10$, $\epsilon_L = 10^{-3}$ and $\epsilon_f = 10^{-2}$. For the SCA method, the convergence parameter is $\epsilon_s = 10^{-2}$. All results are averaged over 50 independent channel realizations.

The convergence of the proposed algorithms for different different values of the distance d_{tk} between the BS transmit MA array and the users, d_{tk} , is shown in Fig. 2. In general, both of the proposed schemes require a relatively low number of iterations to converge. When the users are up to 20 m away from the BS transmit MAs, the ZF-MA scheme achieves a larger WSR than the LP-MA scheme. Since the considered users' channels are modeled similarly as pure line-of-sight (LOS) channels and users are not placed close to each other, the influence of multi-user interference very limited. Additionally, the inter-antenna interference between the receive MAs of a single user is relatively weak for users placed in the vicinity of the BS. Therefore, we can conclude that for MA-enabled ISAC systems operating in the near field, ZF precoding can achieve a larger WSR in the inference limited case. On the other hand, for larger d_{tk} , the LP-

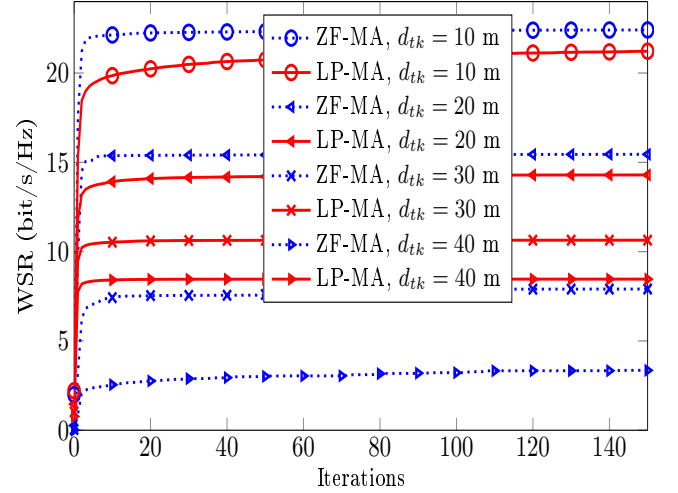


Fig. 2: Convergence of the proposed algorithms for different d_{tk} .

MA scheme provides better WSR performance. In this scenario, the inter-antenna interference between the receive MAs of a single user is increased and the appropriate channel matrices are ill-conditioned (i.e., the corresponding condition numbers are large). Hence, the LP-MA scheme performs an unequal power allocation among different users' precoding matrices, as well as among different sub-channels of the same user, which is the optimal WSR achieving strategy in this case (i.e., waterfilling power allocation). In contrast, the ZF-MA scheme forms a transmission system of orthogonal sub-channels with the equal power gain (i.e., $\mathbf{H}_e \mathbf{P}_e = \beta_e \mathbf{I}_{KN_u}$), resulting in worse system performance for larger d_{tk} .

The WSR for different values of the users rate weights is presented in Fig. 3, where we have imposed the condition $w_1 + w_2 = 1$. The ZF-MA scheme achieves almost constant WSR irrespective of the weighted rate contributions of both users. This is most likely caused by the fact that ZF precoding creates a system of orthogonal sub-channels with equal power gain, and consequently approximately equal achievable rate for every sub-channel. Since both users have the same number of antennas (i.e., sub-channels), any change of the users' weight rates has a negligible influence on the WSR. On the other hand, the WSR for the LP-MA scheme is affected to a significantly greater degree by the users' weight rates. The largest WSR is achieved when most of data transmission is allocated to a single user, while the lowest WSR is obtained when the users' weighted rate contributions

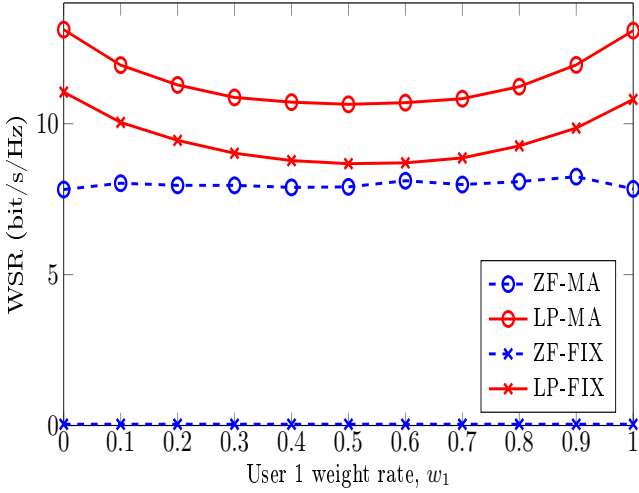


Fig. 3: WSR versus the users' rate weights.

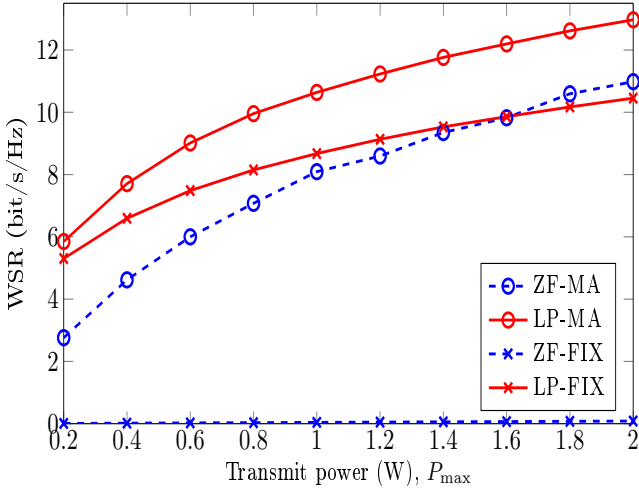


Fig. 4: WSR versus the maximum transmit power.

are approximately equal. This suggests that linear precoding is particularly beneficial in systems with a significant imbalance between the users' rate weights. Regarding the schemes with only fixed antennas, we observe that the LP-FIX scheme achieves around 2 bit/s/Hz lower WSR compared to the LP-MA scheme, while the WSR for the ZF-MA scheme remains negligible for all users' rate weights.

Next, we study how the WSR varies with the maximum transmit power (i.e., P_{\max}), as shown in Fig. 4. The WSR curves for both proposed schemes exhibit an approximately logarithmic shape due to the logarithmic increase in the users achievable rates. Moreover, the performance gap between these two schemes tends to gradually decrease with the transmit power. It seems that the ability of linear precoding to adaptively allocate power offers less WSR advantage for larger transmit powers. A similar effect occurs in conventional point-to-point MIMO systems, where the uniform power allocation becomes optimal at high power levels. The WSR for the LP-FIX scheme is lower than the WSR for the LP-MA scheme and this difference gradually increases with the transmit power. Similarly as in the previous figure, the WSR for the ZF-FIX scheme stays negligibly small irrespective of the transmit power level.

In Fig. 5, we present the WSR for different numbers of MAs at each user. For low N_k , when the inter-antenna interference between different MAs of a single user is relatively small, the ZF-MA scheme provides the best WSR performance. Interestingly,

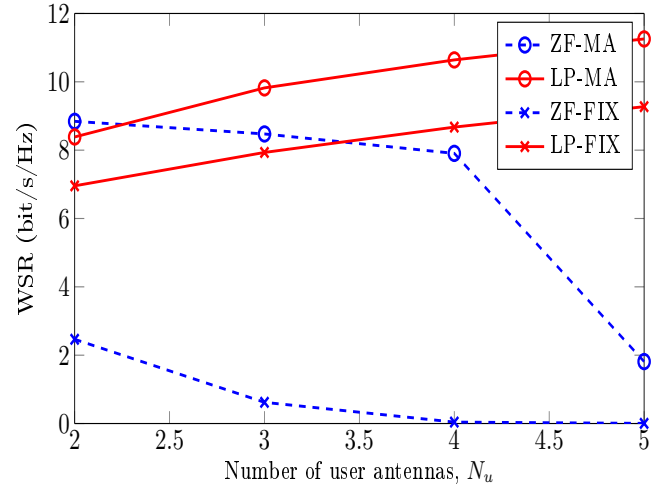


Fig. 5: WSR versus the number of user antennas.

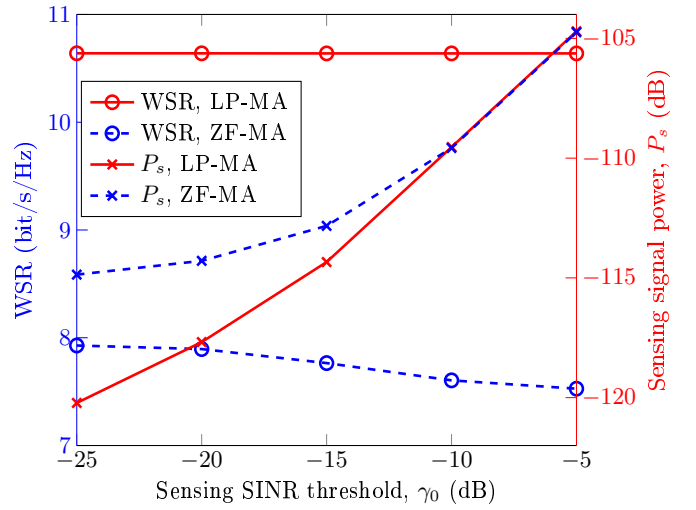


Fig. 6: WSR and sensing signal power versus the sensing SINR threshold.

even the ZF-FIX scheme is capable of providing a moderate WSR, albeit lower than other schemes. However, for larger N_k , the aforementioned interference is increased, leading to a reduction in the WSR for these two schemes. This reduction can be quite severe, as can be seen for the WSR for the ZF-MA scheme when N_k changes from 4 to 5. In contrast to this, the WSRs for the LP-MA and the LP-FIX scheme steadily increase with N_k , due to the ability of linear precoding to adaptively allocate transmit power. This suggests that linear precoding can be particularly useful for future communication systems, where users' terminals are expected to be equipped with a large number of antennas.

In Fig. 6, we show the WSR and the sensing signal power P_s versus the sensing SINR threshold γ_0 . In general, we notice that the considered sensing metric is far more sensitive to the change of the sensing SINR threshold compared the considered communication metric for both schemes. More precisely, the WSR for the ZF-MA scheme drops by only 0.4 bits/s/Hz, while for the LP-MA scheme it remains almost unchanged. On the other hand, the sensing signal powers for the LP-MA and the ZF-MA schemes are changed by approximately 10 dB and 15 dB, respectively. It is also noteworthy that the ZF-MA scheme achieves a moderately larger signal sensing power compared to the LP-MA scheme for low γ_0 , while for larger γ_0 the signal sensing powers of these two schemes are approximately equal.

VI. CONCLUSION

In this paper, we studied the optimization of the WSR in an MA-assisted ISAC system operating in the near field with MAs placed at the BS transmitter and users. To solve this problem, we developed AO-based algorithms that alternately optimize the sensing receive combiner, the communication precoding matrices, the sensing transmit beamformer, the positions of the users MAs and the positions of the BS transmit MAs, for the cases of linear and ZF precoding of the communication signal at the BS. The proposed algorithms were also shown to converge in a small number of iterations. Simulation results verified the effectiveness of the proposed schemes in comparison to fixed-antenna benchmark schemes in a near-field ISAC system, particularly for the scheme with ZF precoding. The largest WSR for the scheme with linear precoding is obtained for the unbalanced users rate weights, while the WSR for the scheme with ZF precoding is almost constant for all users rate weights. We demonstrated that ZF precoding can provide a superior WSR performance for a low number of MAs per user, when the interference between the responses of different users MAs is limited. For a larger number of MAs per user, linear precoding provides a better WSR because of its ability to adaptively allocate transmit power. Finally, it can be observed that the sensing SINR threshold has a significantly greater influence on the sensing than on the communication features of ISAC.

APPENDIX A PROOF OF LEMMA 1

The communication rate of user k can be rewritten as

$$R_{L,k} = \ln |\mathbf{A}_1| - \ln |\mathbf{A}_{2,k}|, \quad (71)$$

where $\mathbf{A}_1 = \sum_{u=1}^K \mathbf{H}_k \mathbf{W}_u \mathbf{W}_u^H \mathbf{H}_k^H + \mathbf{H}_k \mathbf{v} \mathbf{v}^H \mathbf{H}_k^H + \sigma_k^2 \mathbf{I}_{N_u}$ and $\mathbf{A}_{2,k} = \mathbf{A}_1 - \mathbf{H}_k \mathbf{W}_k \mathbf{W}_k^H \mathbf{H}_k^H$.

Differentiating the terms in the previous expressions, we get

$$\frac{d \ln |\mathbf{A}_1|}{dx_{k,b}} = 2\Re \left(\sum_{m=1}^{N_t} \sum_{b'=1}^{N_u} \mathbf{C}_1(m, b') \frac{dx_{k,b} - x_m}{\|\mathbf{t}_m - \mathbf{q}_{k,b}\|} \frac{d\mathbf{H}_k(b', m)}{dx_{k,b}} \right), \quad (72)$$

$$\frac{d \ln |\mathbf{A}_{2,k}|}{dx_{k,b}} = 2\Re \left(\sum_{m=1}^{N_t} \sum_{b'=1}^{N_u} \mathbf{C}_{2,k}(m, b') \frac{dx_{k,b} - x_m}{\|\mathbf{t}_m - \mathbf{q}_{k,b}\|} \frac{d\mathbf{H}_k(b', m)}{dx_{k,b}} \right). \quad (73)$$

Taking the derivatives with respect to individual coordinates of MA b , we have

$$\frac{d\mathbf{H}_k(b, m)}{dx_{k,b}} = j \frac{2\pi\rho_k}{\lambda} \frac{x_{k,b} - x_m}{\|\mathbf{t}_m - \mathbf{q}_{k,b}\|} e^{j\frac{2\pi}{\lambda}\|\mathbf{t}_m - \mathbf{q}_{k,b}\|}, \quad (74)$$

$$\frac{d\mathbf{H}_k(b, m)}{dy_{k,b}} = j \frac{2\pi\rho_k}{\lambda} \frac{y_{k,b} - y_m}{\|\mathbf{t}_m - \mathbf{q}_{k,b}\|} e^{j\frac{2\pi}{\lambda}\|\mathbf{t}_m - \mathbf{q}_{k,b}\|}. \quad (75)$$

Substituting (74) and (75) into (72) (for $b' = b$), we obtain

$$\frac{1}{dx_{k,b}} \frac{d \ln |\mathbf{A}_1|}{dx_{k,b}} = -\frac{4\pi\rho_k}{\lambda} \times \Im \left(\sum_{m=1}^{N_t} \mathbf{C}_1(m, b) \frac{x_{k,b} - x_m}{\|\mathbf{t}_m - \mathbf{q}_{k,b}\|} e^{j\frac{2\pi}{\lambda}\|\mathbf{t}_m - \mathbf{q}_{k,b}\|} \right) \quad (76)$$

and

$$\frac{1}{dy_{k,b}} \frac{d \ln |\mathbf{A}_1|}{dy_{k,b}} = -\frac{4\pi\rho_k}{\lambda} \times \Im \left(\sum_{m=1}^{N_t} \mathbf{C}_1(m, b) \frac{y_{k,b} - y_m}{\|\mathbf{t}_m - \mathbf{q}_{k,b}\|} e^{j\frac{2\pi}{\lambda}\|\mathbf{t}_m - \mathbf{q}_{k,b}\|} \right). \quad (77)$$

In a similar manner, we have

$$\frac{1}{dx_{k,b}} \frac{d \ln |\mathbf{A}_{2,k}|}{dx_{k,b}} = -\frac{4\pi\rho_k}{\lambda} \times$$

$$\Im \left(\sum_{m=1}^{N_t} \mathbf{C}_{2,k}(m, b) \frac{x_{k,b} - x_m}{\|\mathbf{t}_m - \mathbf{q}_{k,b}\|} e^{j\frac{2\pi}{\lambda}\|\mathbf{t}_m - \mathbf{q}_{k,b}\|} \right), \quad (78)$$

$$\frac{1}{dy_{k,b}} \frac{d \ln |\mathbf{A}_{2,k}|}{dy_{k,b}} = -\frac{4\pi\rho_k}{\lambda} \times \Im \left(\sum_{m=1}^{N_t} \mathbf{C}_{2,k}(m, b) \frac{y_{k,b} - y_m}{\|\mathbf{t}_m - \mathbf{q}_{k,b}\|} e^{j\frac{2\pi}{\lambda}\|\mathbf{t}_m - \mathbf{q}_{k,b}\|} \right). \quad (79)$$

Combining the previous expressions, we obtain (35) and (36).

APPENDIX B PROOF OF LEMMA 3

Differentiating the expression (24), we obtain

$$\begin{aligned} d\kappa_l &= d\text{Tr}(\mathbf{u}^H \mathbf{G} \mathbf{M} \mathbf{G}^H \mathbf{u}), \\ &= \text{Tr}(\mathbf{M} \mathbf{G}^H \mathbf{u} \mathbf{u}^H d\mathbf{G} + \mathbf{u} \mathbf{u}^H \mathbf{G} \mathbf{M} d\mathbf{G}^H), \\ &= 2\rho_s \text{Tr}(\mathbf{M} \mathbf{G}^H \mathbf{u} \mathbf{u}^H \mathbf{f}_r d\mathbf{f}_t^H + \mathbf{f}_r^H \mathbf{u} \mathbf{u}^H \mathbf{G} \mathbf{M} d\mathbf{f}_t), \\ &= 2\rho_s \Re \left(\sum_{i=1}^{N_t} \mathbf{e}(i) d\mathbf{f}_t(i) \right). \end{aligned} \quad (80)$$

For the m -th transmit MA, the previous expression is equal to

$$\begin{aligned} d\kappa_l &= 2\rho_s \Re(\mathbf{e}(m) d\mathbf{f}_t(m)) \\ &= -\frac{4\pi\rho_s}{\lambda} \Im \left(\mathbf{e}(m) e^{j\frac{2\pi}{\lambda}\|\mathbf{t}_m - \mathbf{s}_l\|} d\|\mathbf{t}_m - \mathbf{s}_l\| \right) \end{aligned} \quad (81)$$

and from this we can easily obtain (49) and (50).

APPENDIX C PROOF OF LEMMA 4

Differentiating the achievable rate of user k , we obtain

$$dR_{Z,k} = \text{Tr}(\mathbf{F}_k^{-1}) d\beta_e^2 + \text{Tr}((\mathbf{F}_k^{-1} - \mathbf{E}_k^{-1}) d(\mathbf{H}_k \mathbf{v} \mathbf{v}^H \mathbf{H}_k^H)). \quad (82)$$

For the first term on the right-hand side of (82), we have

$$\begin{aligned} \text{Tr}(\mathbf{F}_k^{-1}) d\beta_e^2 &= \text{Tr}(\mathbf{F}_k^{-1}) P_{\max} dT^{-1}, \\ &= P_{\max} T^{-2} \text{Tr}(\mathbf{F}_k^{-1}) \text{Tr}((\mathbf{H}_e \mathbf{H}_e^H)^{-2} d(\mathbf{H}_e \mathbf{H}_e^H)), \\ &= P_{\max} T^{-2} \text{Tr}(\mathbf{F}_k^{-1}) \text{Tr}(\mathbf{B}_e d\mathbf{H}_e + \mathbf{B}_e^H d\mathbf{H}_e^H), \\ &= P_{\max} T^{-2} \text{Tr}(\mathbf{F}_k^{-1}) 2\Re \left(\sum_{m=1}^{N_t} \sum_{k'=1}^K \sum_{b'=1}^{N_k} \mathbf{B}_e(m, b'_k) d\mathbf{H}_e(b'_k, m) \right), \end{aligned} \quad (83)$$

where $b'_k = (k' - 1)N_k + b'$.

For the second term on the right-hand side of (82), we have

$$\begin{aligned} \text{Tr}((\mathbf{F}_k^{-1} - \mathbf{E}_k^{-1}) d(\mathbf{H}_k \mathbf{v} \mathbf{v}^H \mathbf{H}_k^H)) &= \text{Tr}((\mathbf{F}_k^{-1} - \mathbf{E}_k^{-1}) (d\mathbf{H}_k \mathbf{v} \mathbf{v}^H \mathbf{H}_k^H + \mathbf{H}_k \mathbf{v} \mathbf{v}^H d\mathbf{H}_k^H)), \\ &= \text{Tr}(\mathbf{G}_k d\mathbf{H}_k + \mathbf{G}_k^H d\mathbf{H}_k^H), \\ &= 2\Re \left(\sum_{m=1}^{N_t} \sum_{b'=1}^{N_u} \mathbf{G}_k(m, b') d\mathbf{H}_k(b', m) \right). \end{aligned} \quad (84)$$

Taking the derivatives with respect to coordinates of the b -th MA of user k , we have

$$\frac{d\mathbf{H}_k(b, m)}{dx_{k,b}} = j \frac{2\pi\rho_k}{\lambda} \frac{x_{k,b} - x_m}{\|\mathbf{t}_m - \mathbf{q}_{k,b}\|} e^{j\frac{2\pi}{\lambda}\|\mathbf{t}_m - \mathbf{q}_{k,b}\|}, \quad (85)$$

$$\frac{d\mathbf{H}_k(b, m)}{dy_{k,b}} = j \frac{2\pi\rho_k}{\lambda} \frac{y_{k,b} - y_m}{\|\mathbf{t}_m - \mathbf{q}_{k,b}\|} e^{j\frac{2\pi}{\lambda}\|\mathbf{t}_m - \mathbf{q}_{k,b}\|}. \quad (86)$$

Substituting (85) and (86) into (83) and (84) (for $b' = b$), respectively, we obtain that the gradients of R_k w.r.t. the coordinates of the b -th MA of user k are given by (62) and (63).

For the achievable rate of another user $u \neq k$, we have

$$dR_u = \text{Tr}(\mathbf{F}_u^{-1} d\beta_e^2). \quad (87)$$

Repeating the same steps as in (83), we obtain (62) and (63). This completes the proof.

APPENDIX D
PROOF OF LEMMA 5

Differentiating the expression (56), we get

$$\begin{aligned} d\kappa_z &= d(\mathbf{u}^H \mathbf{G}(\gamma_0 \mathbf{P}_e \mathbf{P}_e^H - \mathbf{v}\mathbf{v}^H) \mathbf{G}^H \mathbf{u}), \\ &= \gamma_0 d(\beta_e^2 \mathbf{u}^H \mathbf{G} \mathbf{P}_1 \mathbf{P}_1^H \mathbf{G}^H \mathbf{u}), \\ &= \gamma_0 \mathbf{u}^H \mathbf{G} \mathbf{P}_1 \mathbf{P}_1^H \mathbf{G}^H \mathbf{u} d\beta_e^2 + \gamma_0 \beta_e^2 \text{Tr}(\mathbf{u}^H \mathbf{G} d(\mathbf{P}_1 \mathbf{P}_1^H) \mathbf{G}^H \mathbf{u}), \\ &= \gamma_0 \mathbf{u}^H \mathbf{G} \mathbf{P}_1 \mathbf{P}_1^H \mathbf{G}^H \mathbf{u} d\beta_e^2 + \gamma_0 \beta_e^2 2\Re(\text{Tr}(\mathbf{D}d\mathbf{P}_1)). \end{aligned} \quad (88)$$

Using the derivations from (83), we obtain

$$\begin{aligned} \gamma_0 \mathbf{u}^H \mathbf{G} \mathbf{P}_1 \mathbf{P}_1^H \mathbf{G}^H \mathbf{u} d\beta_e^2 &= \gamma_0 \mathbf{u}^H \mathbf{G} \mathbf{P}_1 \mathbf{P}_1^H \mathbf{G}^H \mathbf{u} \\ &\times 2\Re \left(\sum_{m=1}^{N_t} \sum_{k'=1}^K \sum_{b'=1}^{N_u} \mathbf{B}_e(m, b'_k) d\mathbf{H}_e(b'_k, m) \right). \end{aligned} \quad (89)$$

where $b'_k = (k' - 1)N_k + b'$. Substituting (85) and (86) into the previous expression (for $k' = k$ and $b' = b$), we obtain the first terms on the right-hand side of (64) and (65), respectively.

For the second term in (88), we have

$$\begin{aligned} \gamma_0 \beta_e^2 2\Re(\text{Tr}(\mathbf{D}d\mathbf{P}_1)) &= \gamma_0 \beta_e^2 2\Re(\text{Tr}(\mathbf{D}d\mathbf{H}_e^H (\mathbf{H}_e \mathbf{H}_e^H)^{-1} + \mathbf{D}\mathbf{H}_e^H d(\mathbf{H}_e \mathbf{H}_e^H)^{-1})), \\ &= \gamma_0 \beta_e^2 2\Re(\text{Tr}((\mathbf{H}_e \mathbf{H}_e^H)^{-1} \mathbf{D}d\mathbf{H}_e^H \\ &\quad - \mathbf{D}\mathbf{H}_e^H (\mathbf{H}_e \mathbf{H}_e^H)^{-2} d(\mathbf{H}_e \mathbf{H}_e^H))), \\ &= \gamma_0 \beta_e^2 2\Re(\text{Tr}(-\mathbf{H}_e^H \mathbf{D}\mathbf{H}_e^H (\mathbf{H}_e \mathbf{H}_e^H)^{-2} d\mathbf{H}_e \\ &\quad + [(\mathbf{H}_e \mathbf{H}_e^H)^{-1} \mathbf{D} - \mathbf{D}\mathbf{H}_e^H (\mathbf{H}_e \mathbf{H}_e^H)^{-2} \mathbf{H}_e] d\mathbf{H}_e^H)), \\ &= \gamma_0 \beta_e^2 2\Re(\text{Tr}(-\mathbf{D}_1 d\mathbf{H}_e + \mathbf{D}_2^T d\mathbf{H}_e^*)), \\ &= \gamma_0 \beta_e^2 \sum_{m=1}^{N_t} \sum_{k'=1}^K \sum_{b'=1}^{N_u} 2\Re(-\mathbf{D}_1(m, b'_k) d\mathbf{H}_e(b'_k, m) \\ &\quad + \mathbf{D}_2^T(m, b'_k) d\mathbf{H}_e^*(b'_k, m)). \end{aligned} \quad (90)$$

Substituting (85) and (86) into the previous expression (for $k' = k$ and $b' = b$), we obtain the second terms on the right-hand side of (64) and (65), respectively. This completes the proof.

REFERENCES

- [1] N. S. Perović, K. Singh, C.-P. Li, and M. F. Flanagan, "Weighted sum rate optimization for movable antenna enabled near-field ISAC," *arXiv preprint arXiv:2510.19759*, 2025.
- [2] F. Liu, Y. Cui, C. Masouros, J. Xu, T. X. Han, Y. C. Eldar, and S. Buzzi, "Integrated sensing and communications: Toward dual-functional wireless networks for 6G and beyond," *IEEE J. Sel. Areas Commun.*, vol. 40, no. 6, pp. 1728–1767, 2022.
- [3] N. S. Perović, M. F. Flanagan, and L.-N. Tran, "Sensing rate optimization for multi-band cooperative ISAC systems," *IEEE Commun. Lett.*, vol. 29, no. 9, pp. 2163–2167, 2025.
- [4] A. Magbool, V. Kumar, Q. Wu, M. Di Renzo, and M. F. Flanagan, "A survey on integrated sensing and communication with intelligent metasurfaces: Trends, challenges, and opportunities," *IEEE open j. Commun. Soc.*, vol. 6, 2025.
- [5] K. Rojith, R. Allu, K. Singh, K. Dev, and S. Biswas, "Optimizing uplink multi-user performance in ISAC system with RFID backscatter," in *Proc. IEEE ICC*, 2025, pp. 1–6.
- [6] P. Saikia, A. Jee, K. Singh, T. A. Tsiftsis, and A.-A. A. Boulogeorgos, "Hybrid-RIS empowered UAV-aided ISAC systems," in *Proc. IEEE VTC-Fall*, 2024, pp. 1–5.
- [7] S. Mondal, K. Singh, D. W. K. Ng, C.-P. Li, and Z. Ding, "Outage performance of RIS-aided NOMA ISAC network for LEO satellite system," in *Proc. IEEE ICC Workshops*, 2025, pp. 1556–1561.
- [8] F. Liu, C. Masouros, A. P. Petropulu, H. Griffiths, and L. Hanzo, "Joint radar and communication design: Applications, state-of-the-art, and the road ahead," *IEEE Trans. Commun.*, vol. 68, no. 6, pp. 3834–3862, 2020.
- [9] M. S. Ibrahim, A. Konar, and N. D. Sidiropoulos, "Fast algorithms for joint multicast beamforming and antenna selection in massive MIMO," *IEEE Trans. Signal Process.*, vol. 68, pp. 1897–1909, 2020.
- [10] S. Yang, B. Liu, Z. Hong, and Z. Zhang, "Low-complexity sparse array synthesis based on off-grid compressive sensing," *IEEE Antennas Wirel. Propag. Lett.*, vol. 21, no. 12, pp. 2322–2326, 2022.
- [11] F. Liu, Y. Liu, K. Da Xu, Y.-L. Ban, Q. H. Liu, and Y. J. Guo, "Synthesizing uniform amplitude sparse dipole arrays with shaped patterns by joint optimization of element positions, rotations and phases," *IEEE Trans. Antennas Propag.*, vol. 67, no. 9, pp. 6017–6028, 2019.
- [12] S. P. Chepuri, N. Shlezinger, F. Liu, G. C. Alexandropoulos, S. Buzzi, and Y. C. Eldar, "Integrated sensing and communications with reconfigurable intelligent surfaces: From signal modeling to processing," *IEEE Signal Process. Mag.*, vol. 40, no. 6, pp. 41–62, 2023.
- [13] K. Zhong, J. Hu, C. Pan, M. Deng, and J. Fang, "Joint waveform and beamforming design for RIS-aided ISAC systems," *IEEE Signal Process. Lett.*, vol. 30, pp. 165–169, 2023.
- [14] X. Qian, X. Hu, C. Liu, M. Peng, and C. Zhong, "Sensing-based beamforming design for joint performance enhancement of RIS-aided ISAC systems," *IEEE Trans. Commun.*, vol. 71, no. 11, pp. 6529–6545, 2023.
- [15] X. Yang, Z. Wei, Y. Liu, H. Wu, and Z. Feng, "RIS-assisted cooperative multicell ISAC systems: A multi-user and multi-target case," *IEEE Trans. Wireless Commun.*, vol. 23, no. 8, pp. 8683–8699, 2024.
- [16] Q. Zhu, M. Li, R. Liu, and Q. Liu, "Joint transceiver beamforming and reflecting design for active RIS-aided ISAC systems," *IEEE Trans. Veh. Technol.*, vol. 72, no. 7, pp. 9636–9640, 2023.
- [17] L. Zhu, W. Ma, and R. Zhang, "Movable antennas for wireless communication: Opportunities and challenges," *IEEE Commun. Mag.*, vol. 62, no. 6, pp. 114–120, 2023.
- [18] L. Zhu, W. Ma, W. Mei, Y. Zeng, Q. Wu, B. Ning, Z. Xiao, X. Shao, J. Zhang, and R. Zhang, "A tutorial on movable antennas for wireless networks," *IEEE Commun. Surv. Tutor.*, 2025.
- [19] W. Ma, L. Zhu, and R. Zhang, "Movable antenna enhanced wireless sensing via antenna position optimization," *IEEE Trans. Wireless Commun.*, vol. 23, no. 11, pp. 16575–16589, 2024.
- [20] L. Chen, M.-M. Zhao, M.-J. Zhao, and R. Zhang, "Antenna position and beamforming optimization for movable antenna enabled ISAC: Optimal solutions and efficient algorithms," *arXiv preprint arXiv:2502.14198*, 2025.
- [21] W. Lyu, S. Yang, Y. Xiu, Z. Zhang, C. Assi, and C. Yuen, "Movable antenna enabled integrated sensing and communication," *IEEE Trans. Wireless Commun.*, vol. 24, no. 4, pp. 2862–2875, 2025.
- [22] C. Jiang, C. Zhang, C. Huang, J. Ge, D. Niyato, and C. Yuen, "Movable antenna-assisted integrated sensing and communication systems," *IEEE Trans. Wireless Commun.*, vol. 24, no. 8, pp. 6397–6412, 2025.
- [23] R. Yang, Z. Dong, P. Cheng, W. Lyu, Y. Xiu, Y. Li, and N. Wei, "Robust transceiver design for RIS enhanced dual-functional radar-communication with movable antenna," *arXiv preprint arXiv:2506.07610*, 2025.
- [24] A. Khalili and R. Schober, "Advanced ISAC design: Movable antennas and accounting for dynamic RCS," in *Proc. IEEE GLOBECOM*, 2024, pp. 4022–4027.
- [25] Z. Kuang, W. Liu, C. Wang, Z. Jin, J. Ren, X. Zhang, and Y. Shen, "Movable-antenna array empowered isac systems for low-altitude economy," in *Proc. IEEE ICC*, 2024, pp. 776–781.
- [26] Y. Liu, Z. Wang, J. Xu, C. Ouyang, X. Mu, and R. Schober, "Near-field communications: A tutorial review," *IEEE Open J. Commun. Soc.*, vol. 4, pp. 1999–2049, 2023.
- [27] J. An, C. Yuen, L. Dai, M. Di Renzo, M. Debbah, and L. Hanzo, "Near-field communications: Research advances, potential, and challenges," *IEEE Wireless Commun.*, vol. 31, no. 3, pp. 100–107, 2024.
- [28] Y. Sun, H. Xu, C. Ouyang, and H. Yang, "Rotatable and movable antenna-enabled near-field integrated sensing and communication," *arXiv preprint arXiv:2501.04490*, 2025.
- [29] J. Ding, Z. Zhou, X. Shao, B. Jiao, and R. Zhang, "Movable antenna-aided near-field integrated sensing and communication," *IEEE Trans. Wireless Commun.*, 2025, early access.
- [30] R. Zhang, J. Ding, Q. Zhou, J. Wang, Y. Gong, and A. Nallanathan, "Deep learning-driven MA-RIS co-design for near-field ISAC: Joint antenna positioning, phase shifting and beamforming optimization," *IEEE Trans. Cogn. Commun. Netw.*, 2025, early access.
- [31] Z. He, W. Xu, H. Shen, D. W. K. Ng, Y. C. Eldar, and X. You, "Full-duplex communication for ISAC: Joint beamforming and power optimization," *IEEE J. Sel. Areas Commun.*, vol. 41, no. 9, pp. 2920–2936, 2023.
- [32] Z. Zhang, Z. Zhao, K. Shen, D. P. Palomar, and W. Yu, "Discerning and enhancing the weighted sum-rate maximization algorithms in communications," *arXiv preprint arXiv:2311.04546*, 2023.
- [33] S. Le Cleach, M. Schwager, and Z. Manchester, "Algames: a fast augmented Lagrangian solver for constrained dynamic games," *Autonomous Robots*, vol. 46, no. 1, pp. 201–215, 2022.
- [34] F. Dong, F. Liu, Y. Cui, W. Wang, K. Han, and Z. Wang, "Sensing as a service in 6G perceptive networks: A unified framework for ISAC resource allocation," *IEEE Trans. Wireless Commun.*, vol. 22, no. 5, pp. 3522–3536, 2022.